P-06-54

A comparison between standard well test evaluation methods used in SKB's site investigations and the generalised radial flow concept

Sven Follin, SF GeoLogic AB

Jan-Erik Ludvigson, Jakob Levén
Geosigma AB

September 2011

Svensk Kärnbränslehantering AB
Swedish Nuclear Fuel
and Waste Management Co

Box 250, SE-101 24 Stockholm
Phone +46 8 459 84 00

ISSN 1651-4416
SKB P-06-54

A comparison between standard well test evaluation methods used in SKB's site investigations and the generalised radial flow concept

Sven Follin, SF GeoLogic AB

Jan-Erik Ludvigson, Jakob Levén
Geosigma AB

September 2011

Keywords: SKBdoc 1297358, Forsmark, Hydrogeology, Hydraulic tests, Injection tests, Difference flow logging.

Preface

The analyses presented in this report were completed in 2006, and the written report has been finalised in 2011. Despite the gap in time, the written report does not reflect any work beyond the effort of 2006. The significant results of the analyses were available to the site descriptive modelling at Forsmark, and were transferred to higher-level studies in time for groundwater flow modelling of the complete site investigation phase. Hence, we do not believe the results of this investigation affect or alter the conclusions of site assessment activities that support site selection or licensing.

September 2011

Sven Follin

SF GeoLogic AB

Abstract

According to the strategy for hydrogeological characterisation within the SKB's site investigation programme, two single-hole test methods are available for testing and parameterisation of groundwater flow models – constant-head injection testing with the Pipe String System (PSS method) and difference flow logging with the Posiva Flow Log (PFL method). This report presents the results of an investigation to assess discrepancies in the results of single-hole transmissivity measurements using these methods in the Forsmark site characterisation. The investigation explores the possibility that the source of the discrepancy observed lies in the assumptions of the flow geometry that are inherent to the methods used for standard constant-head injection well test analysis and difference flow logging analysis, respectively. In particular, the report looks at the generalised radial flow (GRF) concept by Barker (1988) as a means that might explain some of the differences. A confirmation of the actual flow geometries (dimensions) observed during hydraulic injection tests could help to identify admissible conceptual models for the tested system, and place the hydraulic testing with the PSS and PFL test methods in its full hydrogeological context.

The investigation analyses 151 constant-head injection tests in three cored boreholes at Forsmark. The results suggest that the transmissivities derived with standard constant-head injection well test analysis methods and with the GRF concept, respectively, are similar provided that the dominating flow geometry during the testing is radial (cylindrical). Thus, having flow geometries with dimensions other than 2 affects the value of the interpreted transmissivity. For example, a flow system with a dimension of 1 may require an order of magnitude or more, higher transmissivity to produce the same flow rates. The median of the GRF flow dimensions of all 151 constant-head injection tests is 2.06 with 33% of the tests in the range 1.75–2.25, 40% in the range 2.25–3, and 27% in the range 0–1.75. It is noted that transmissivity is by definition a two-dimensional quantity and that values derived from tests with flow dimensions less than 1 and greater than 3 are not readily implemented as fracture transmissivities in discrete fracture network flow models. If the 11 tests with flow dimensions less than 1 are excluded, the changes in the statistics are insignificant; the median becomes 2.16 with 35% of the tests in the range 1.75–2.25, 44% in the range 2.25–3, and 21% in the range 1–1.75.

In conclusion, the discrepancies seen in the results of single-hole transmissivity measurements using the PSS and PFL methods predominantly reflect the fact that PFL measurements are taken after several days of pumping, whereas PSS measurements are recording 20 min of response after test interval perturbation. Indeed, a test interval intersecting a finite fracture or network may produce a flow in the early time period of the PSS test, but record a reduced or no flow by the time running of the PFL tool. This conclusion is supported by the pressure recoveries observed after injection shut-in, where several of the constant-head injection tests that have a flow dimension less than 1 have also an incomplete pressure recovery. Hence, one might expect a discrepancy in a cross-plot toward lower values in the PFL transmissivities compared with the PSS values. A comparison of the cumulative distributions of the PFL and PSS transmissivities for one of the investigated boreholes indicates that deviations start at about $5 \cdot 10^{-8}$ m^2/s, and that PSS transmissivities are generally greater than PFL transmissivities below this value.

Sammanfattning

Injektionstester har varit standardmetoden för SKB:s hydrotester i berg sedan början på 1980-talet. I samband med platsundersökningarna i Forsmark och Simpevarp/Laxemar började SKB även använda differensflödesloggning under pumpning. Föreliggande rapport undersöker om det är olikheter i flödesgeometri och/eller utvärderingsmetodik som är anledningen till varför transmissiviteter tolkade med injektionstester (PSS) ibland skiljer sig från transmissiviteter tolkade med flödesloggning (PFL). Specifikt undersöks hur utvärderingen av flödesgeometri och transmissivitet enligt teorin för generaliserat radiellt flöde (Barker 1988) jämför sig med utvärderingen av flödesgeometri och transmissivitet enligt de standardmetoder som SKB traditionellt använder sig av för att tolka injektionstester.

Rapporten redovisar resultat från 151 injektiontester i tre kärnborrhål i Forsmark. GRF analyserna ger 2.06 som ett medianvärde på flödesdimensionen, där 33 % av testerna har en flödesdimension i intervallet 1.75–2.25, 40 % i intervallet 2.25–3 och 27 % i intervallet 0–1.75. Om man exkluderar tester med en flödesdimension mindre än 1 med motivet att transmissivitet är en tvådimensionell storhet, ändras antalet tester i analysen till 140 och medianvärdet ändras till 2.16, med 35 % av testerna i intervallet 1.75–2.25, 44 % i intervallet 2.25–3 och 21 % i intervallet 1–1.75.

Sammanfattningvis konstateras att huvudorsaken till att transmissiviteter tolkade med flödesloggning ibland skiljer sig från transmissiviteter tolkade med injektionstester beror på att mätningarna vid flödesloggning sker efter flera dagars pumpning medan mätningarna vid injektionstester pågår endast under 20 minuter. Att 20 minuter långa injektionstester kan resultera i höga transmissiviteter fastän spricknätverket är dåligt konnekterat bekräftas av dålig tryckåterhämtning efter avslutad injektionstest; flera av de anlyserade injektionstesterna med låg flödesdimension har också visat sig ha en dålig tryckåterhämtning. Man ska med andra ord förvänta sig att data i ett korsdiagram med transmissiviteter tolkade med flödesloggning på den ena axeln och transmissiviteter tolkade med injektionstester på den andra inte alltid faller på en 1:1 linje, i synnerhet inte i det lägre transmissivitetsregistret. En jämförelse av de kumulativa fördelningarna för beräknade PFL och PSS transmissiviteter i ett av de analyserade borrhålen indikerar att skillnader börjar vid ca $5 \cdot 10^{-8}$ m^2/s och att PSS transmissiviteter är i allmänhet större än PFL transmissiviteter under detta värde.

Contents

1 Introduction

1.1 Background

The Swedish Nuclear Fuel and Waste Management Company (SKB) is undertaking site characterisation at two different locations, the Forsmark and Simpevarp/Laxemar areas, with the objective of siting a geological repository for spent nuclear fuel. The site investigations are conducted in campaigns, punctuated by data freezes. After each data freeze, the site data are analysed and modelling is carried out with the overall purpose to develop a site descriptive model (SDM). At the completion of the Forsmark data freeze 2.1, seven cored boreholes, KFM01A–7A, have been hydraulically investigated, see Figure 1-1.

According to the strategy for hydrogeological characterisation within the SKB's site investigation programme, two single-hole test methods are available for testing and parameterisation of groundwater flow models (Rhén et al. 2003) – constant-head injection testing with the Pipe String System (PSS method) and difference flow logging with the Posiva Flow Log (PFL method). Constant-head injection testing with the PSS method has been SKB's standard method for characterisation of flow in fractured bedrock. It was used extensively used in the Swedish programme for nuclear waste disposal prior to the initiation of the site investigation programmes (Almén et al. 1986a b). The PFL

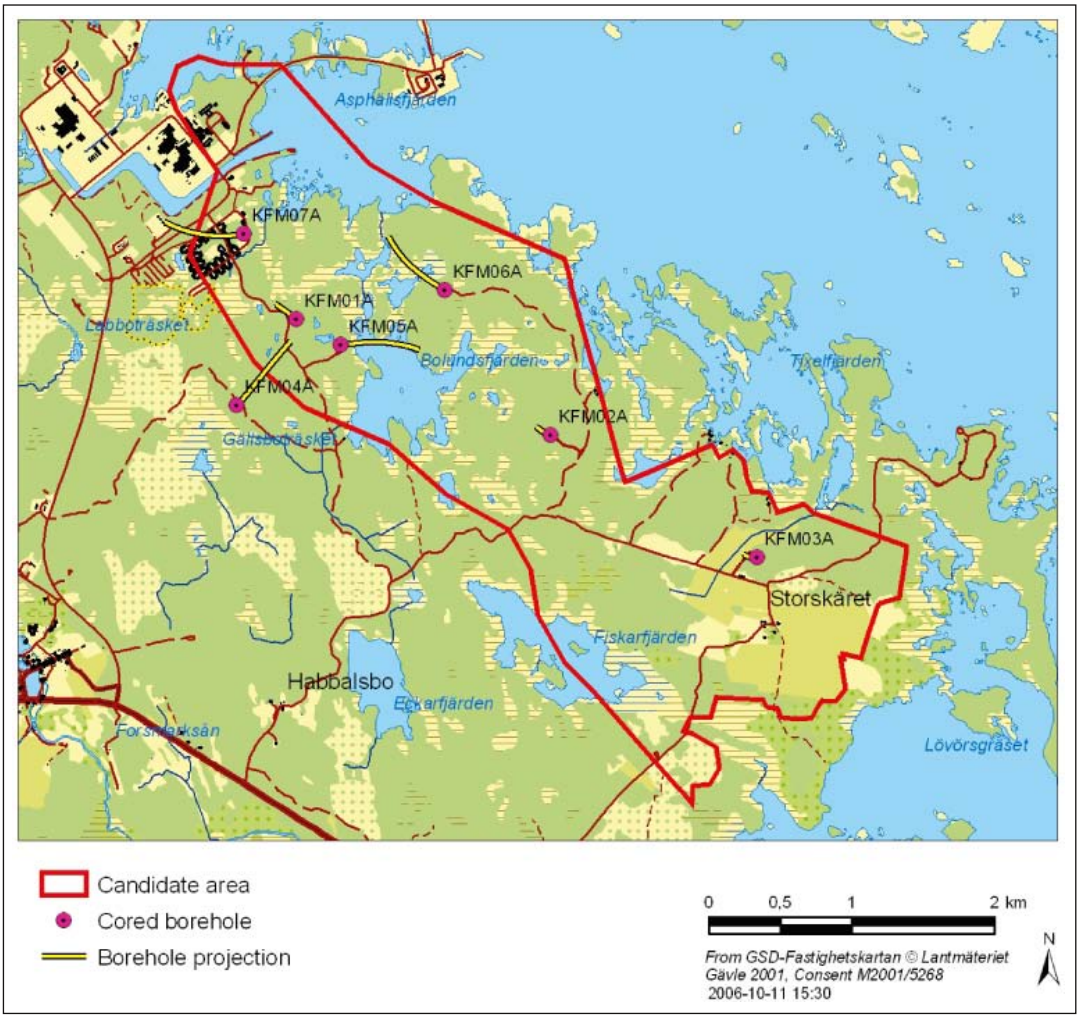

Figure 1-1. *At the completion of the Forsmark data freeze 2.1, seven cored boreholes, KFM01A–7A, are hydraulically investigated. Levén et al. (2006) visualise data from different earth science disciplines for each borehole KFM01A–7A. Data for boreholes KFM02A, KFM03A and KFM06A are shown in Appendix A.*

method is a fairly new test method that came into use about the same time as the site investigation programmes at Simpevarp/Laxemar and Forsmark began (Ludvigson et al. 2002). It was developed by Posiva Oy for usage with the Finnish site characterisation programme, and it has seen virtually no other applications except in the Swedish site characterisation programme. In order to learn more about the advantages and disadvantages of the PFL method the seven boreholes in Figure 1-1 have investigated with both methods.

A key reason for using the PFL method despite its novelty is its significantly shorter operational time in the field and its superior geometrical resolution. For instance, to test a one kilometre long cored borehole with a resolution of 0.1 m between measurements takes about four to seven days in total with the PFL method. In comparison, the total operational time in the field using the PSS method is approximately four weeks and the finest geometrical resolution is 5 m between measurements. (A finer geometrical resolution is of course possible with the PSS method, but that would also imply an even longer total operational time in the field.) Second, an early screening of the frequency and transmissivity of water conducting fractures is an important input to the hydrogeochemical characterisation programme, which needs to decide on the best packer positions for the sampling of fracture water and matrix porewater.

The frequency and transmissivity of water conducting fractures deduced from measurements conducted with the PFL method is of key interest also for the site characterisation and hydrogeological understanding as well as for the subsequent parameterisation of groundwater flow models using the discrete fracture network (DFN) and equivalent continuous porous medium (ECPM) approaches, see Figure 1-2. In the ECPM approach, the underpinning discrete fracture network (DFN) realisation is assigned stochastic transmissivity values based on a statistical analysis of measured PFL and PSS transmissivities, see Follin et al. (2005) and Hartley et al. (2005) for details. Since each ECPM model studied is based on a particular underlying stochastic DFN realisation, the ECPM models are also stochastic. It is noted that in both approaches, DFN and ECPM, the transmissivity values between fractures vary in space in a stochastic fashion but that in every realisation each fracture is considered hydraulically homogeneous.

1.2 Scope and objectives

This report presents the results of an investigation to assess discrepancies seen in the results of single-hole transmissivity measurements using the PSS and PFL methods in the cored boreholes at Forsmark. The investigation explore the possibility that the source of the discrepancy lies in assumptions of the flow geometry that are inherent to the methods used for standard constant-head injection well test analysis and difference flow logging analysis, respectively. Both methods assume two-dimensional radial (cylindrical) flow. In particular, the report looks at the generalised radial flow (GRF) concept (Barker 1988) as a means that might explain some of the differences. A confirmation of the actual flow geometries (dimensions) observed during hydraulic injection tests could help to identify admissible conceptual models for the tested system, and place the hydraulic testing with the PSS and PFL methods in its full hydrogeological context, e.g. whether or not these give different types of information of benefit for the site characterisation and subsequent groundwater flow modelling studies.

There have been some uncertainties as how to explain the deviations from a 1:1 slope seen in cross-plots comparing the PSS and PFL results. Figure 1-3 shows an example from borehole KFM06A. In this plot the PSS transmissivity value of the 5-m test intervals are plotted versus the corresponding lumped transmissivity values of all PFL fracture transmissivities within each 5-m test interval. The measurements shown in Figure 1-3 represent conditions in bedrock outside deformation zones.

Some of the differences seen in the transmissivity results are probably due to operational differences, e.g.:

- injection (PSS) versus pumping (PFL),
- long test interval (PSS) versus short test interval (PFL),
- short-term flow conditions during testing (PSS) versus long-term flow conditions during testing (PFL),
- a robust lower measurement limit (PSS) versus a variable practical lower measurement limit (PFL).

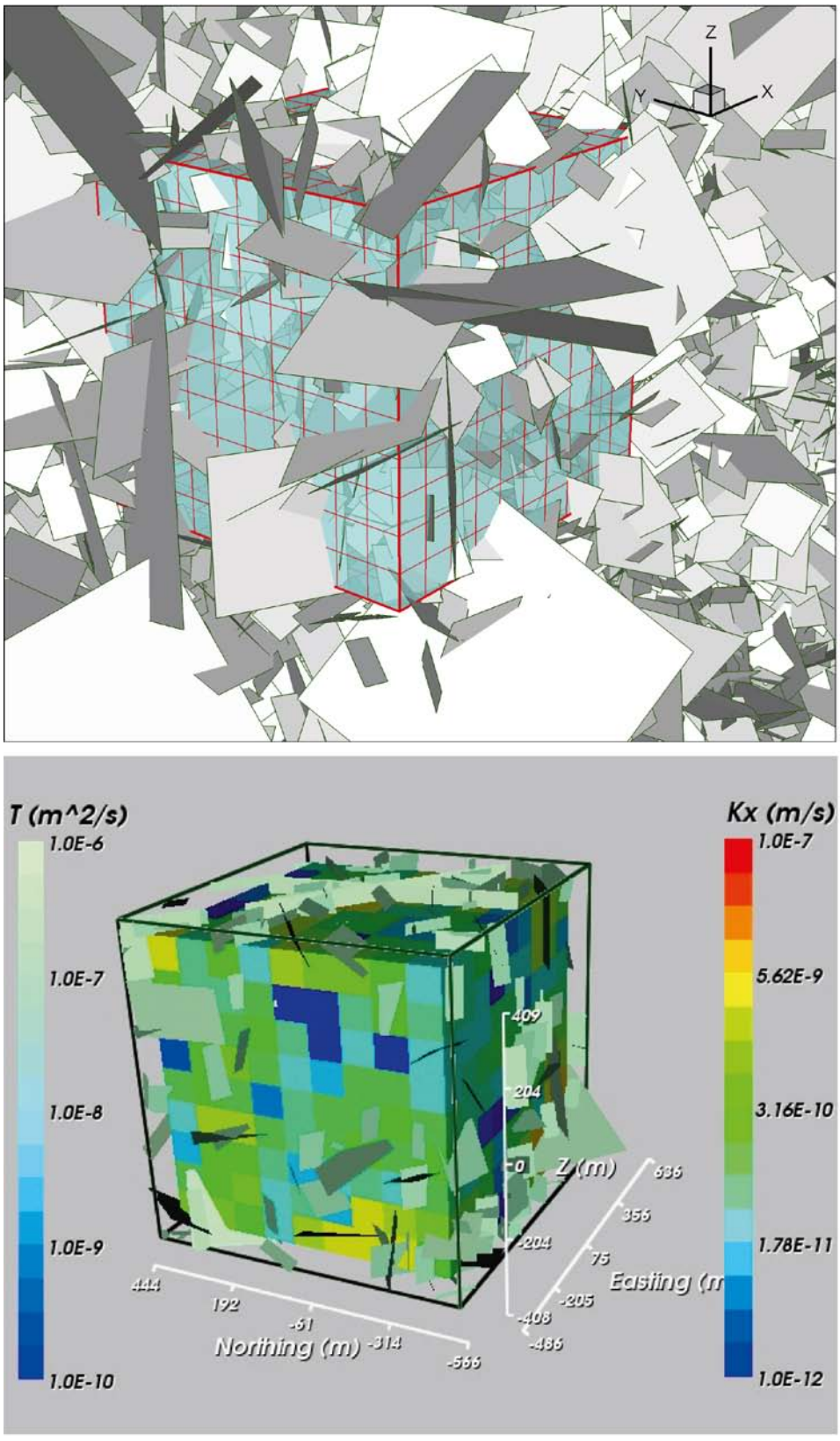

Figure 1-2. *Illustrations showing of the ECPM modelling approach. Geometrical and hydraulic properties of modelled 2D discrete features are transformed into an equivalent continuous porous medium with heterogeneous and anisotropic grid properties in 3-D.*

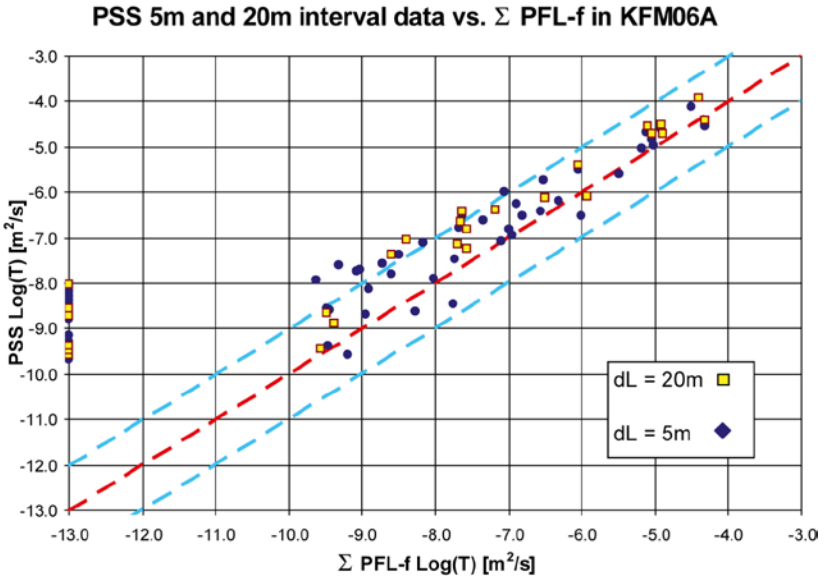

Figure 1-3. *Cross-plot of PSS transmissivity data vs. Σ PFL fracture transmissivity data in borehole KFM06A. The red line indicates a unit slope and the blue lines a spread of ± 1 order of magnitude. Data are shown for two test interval lengths between the PSS packers, 5 m and 20 m. PSS transmissivity data from test intervals without PFL fracture transmissivity data are in this plot shown to the left, i.e., plotted with an arbitrary low value on the abscissa. Values of ΣT_{PFL} above the 1:1 slope are probably due to interpretation or methodological uncertainties as there is risk for double-counting in the calculation of ΣT_{PFL}. For instance, this would occur if two or more intersecting fractures within a 5-m test interval merge to a single fracture away from the borehole.*

Other differences in the results are more subtle, e.g. consequences of the methodologies decided by SKB for single-hole hydraulic test interpretations using injection tests and difference flow logging:

- PSS: Method descriptions SKB MD 323.001[1] and SKB MD 320.004[1]
- PFL: Method description SKB MD 322.010[2]

There are two "standard" approaches for interpreting PSS tests – a steady-flow standard and a transient-flow standard. The more traditional approach assumes steady-flow, that is, the flow rate and pressure do not change with time. PSS tests, which are also known as "packer tests", are mainly used for engineering construction purposes, where steady-flow methods are traditional. Transient methods are more common for well tests that are done for water resource development or petroleum exploration involving higher flow rates and longer open well intervals. There is no reason, however, why transient methods of water and oil development cannot be applied to packer tests. A number of mathematical solutions for analysing transient well test data are in general use. They are mostly developed for porous and not fractured media, and they assume 2D flow from a confined or partially confined sedimentary aquifer, i.e., a geological unit with a reasonably homogeneous conductivity-thickness product (transmissivity) and a large radial (cylindrical) extension. A discussion of why these are or are not applicable to fractured is beyond the scope of this report. Simply stated, the solutions in use for water wells in sedimentary rock are taken as "standard" for the PSS analysis in SKB's site investigation programme and are available in the commercial well test analysis software.

The standard well test analysis methods used for the interpretation of PSS injection tests are described in Ludvigson et al. (2007). The interpreted test interval transmissivity is inferred from the radial-acting transient flow period during 20 minutes of injection (or during the subsequent pressure recovery period following injection shut-in). This period of the response curve is denoted as the "the first radial-acting transient flow period" in the work reported here. The interpretation is considered to yield *representative hydraulic properties* of the hydraulic features penetrated by the borehole and accounts for the impact of wellbore storage and borehole skin.

[1] The essence of this method description is described in Ludvigson et al. (2007).

[2] The essence of this method description is described in Ludvigson et al. (2002).

If a transient evaluation is not possible to carry out with confidence, the derivation of the PSS test interval transmissivity is based on the flow rate and differential pressure at injection shut-in using Moye's formula for steady-state radial flow (Moye 1967), see Section 2.2.2 for details.

By contrast, the PFL method does not collect transient data and the analysis must rely only on steady flow equations for interpreting the transmissivity. As discussed in subsequent sections, the PSS and PFL steady flow analyses do not use the same equations. The steady flow equation for the PSS tests assumes a porous medium where flow becomes spherical near the ends of the test section, that is, pseudo-radial flow geometry is assumed (see Figure 1-4). By comparison, the test interval transmissivity obtained from the PFL method, which assumes a cylindrical flow regime to a line sink, is simply the long-term specific capacity derived from the difference in flow rate divided by difference in head change for two subsequent flow loggings. There are not huge differences between these two steady flow methods, but the differences need to be noted.

The report explores the concept of flow dimension by Barker (1988) by analysing a number of PSS tests conducted in three cored boreholes, KFM02A, KFM03A and KFM06A using the AQTESOLV software (version 4.0, HydroSOLVE, Inc.). Appendix A provides an overview of the multi-disciplinary information available in these boreholes. It is anticipated that the concept of flow dimension may give some hints as to whether the transmissivity of the first radial-acting flow period of the PSS injection tests, implying a flow dimension of 2, adequately represents the spatially varying geometrical and hydraulic properties of the conducting flow paths within the main transmissive features.

1.3 Previous work

Among the first applications of the GRF concept to hydraulic test data acquired in fractured crystalline rock are probably the works by Doe and Geier (1990), Geier et al. (1992, 1996), and Wei and Chakrabarty (1996). In sparsely fractured crystalline rock, a single fracture is often responsible for all the flow observed in a test interval. In such a case, the estimate of transmissivity based on the first radial-acting flow regime may be misleading, particularly if the flow is channelised, see Figure B-1 in Appendix B for an example.

Doe (2002) concludes that the flow dimension of a flowing conductor is readily recognisable from the shape of the well test curve and particularly the shape of the derivative. For instance, for constant-rate tests, the slope of the build-up or draw down curve in logarithmic plots will be equal to (1–n/2) for flow dimensions less than 2. Thus a linear flow conductor (n = 1) will have

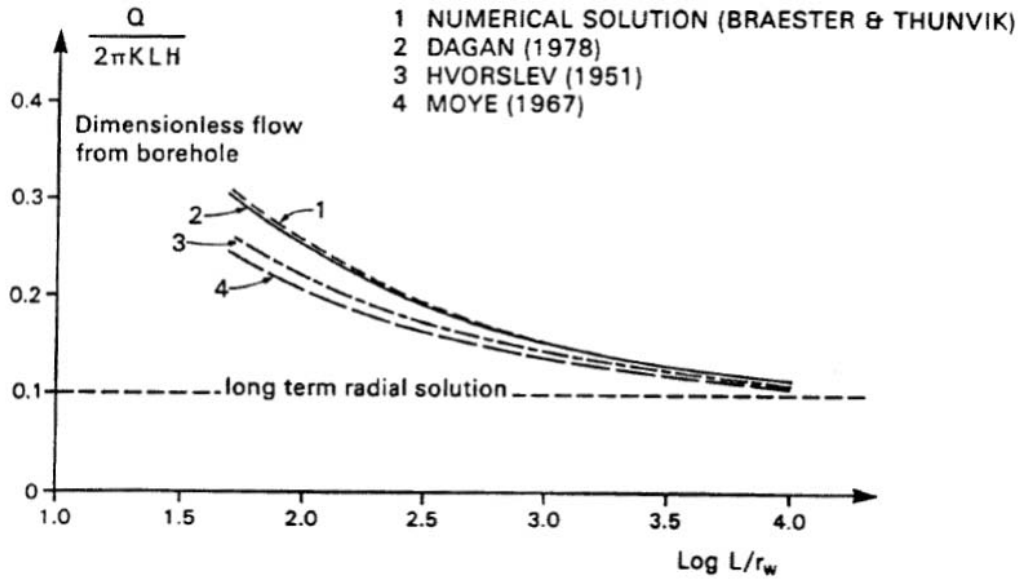

Figure 1-4. *Spherical flow effects as a function of the ratio between the test interval length L and the borehole radius r_w. Reproduced from Black and Barker (1987) who refer to Braester and Thunvik (1982, 1984).*

a characteristic ½ slope. The pressure derivative plot has advantages in dealing with generalised (fractional) dimension flow, because a pressure derivative curve will approach a slope of (1–n/2) for all dimensions including those between 2 and 3.

Figure 1-5 shows the range of pressure derivative curves in a homogeneous and isotropic medium for dimensions where the derivative slope varies from +0.5 to –0.5 for flow dimensions varying from 1 to 3[3]. Non-integer flow dimension systems produce derivative slopes lying between the integer dimension curves (fractional flow). For example, a conductor with a dimension of n = 1.5 will yield a response curve and a derivative with a slope of ¼.

Boundary effects are also very clear in derivative plots. A positive unit-slope in the derivative curve indicates a no-flow boundary, such as the limit of a compartmentalised network of fractures. A steeply dropping derivative (steeper than a –0.5 slope) indicates intersection with a significantly more permeable feature at some distance from the pumping source.

Further, Doe (2002) concludes that well test dimensions exist independently of the nature of the flow geometry (medium). One can conceive both fracture and continuum geometries that will produce identical well test results. Hence, a particular dimension, such as dimension 1 (n = 1), is not by itself an indicator of fracture flow. The flow dimension is simply related to how the conducting area grows with distance regardless if the medium is porous or discrete (fractured).

Heterogeneities may lead to different kind of apparent no-flow boundaries, as reflected from the response derivative, depending on their actual geometries (Follin 1992, Walker and Roberts 2003). Put into practice, this implies that the flow dimension may vary with time during a transient hydraulic test. Flow geometry and parameter heterogeneity are, in fact, continuously interchangeable as interpretations of the flow dimension. In the work reported here, parameter heterogeneity is neglected while the ambition has been to match as much as possible of the entire injection period expressed as a single value of the flow dimension.

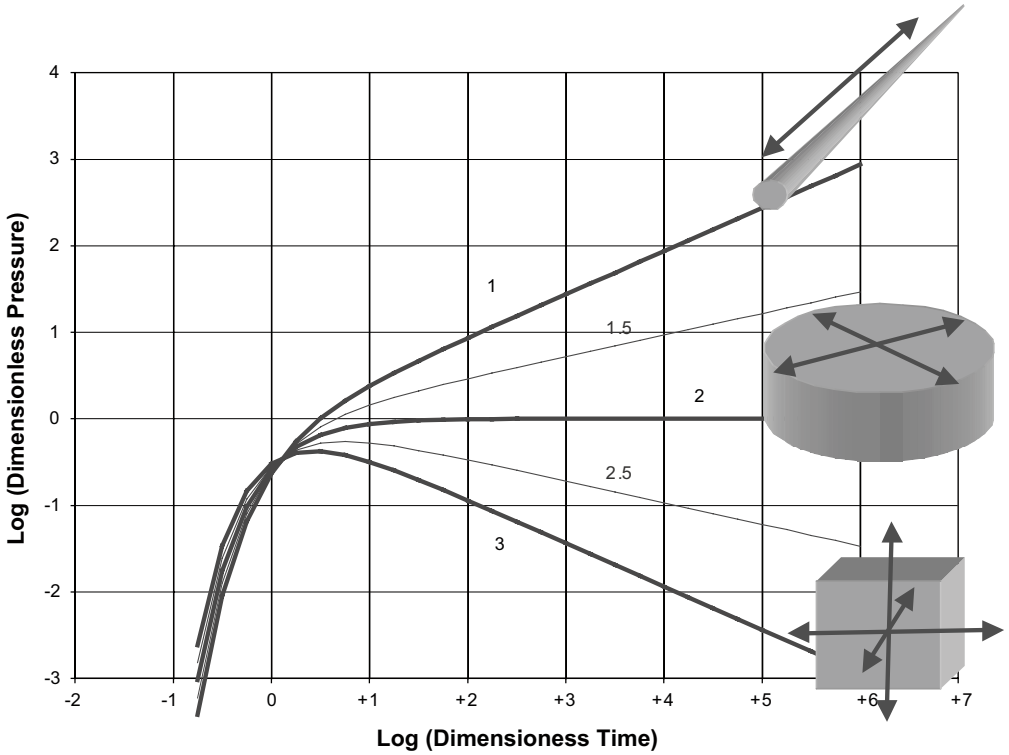

Figure 1-5. *Illustration of flow geometry and pressure derivative curves for constant-rate tests. Numbers on curves indicate flow dimension. (Modified after Doe (2002)). An analogous plot for constant-head tests is presented in Figure 2-2 on p. 13 in Geier et al. (1996).*

[3] Figure 1-5 represents the derivative from a constant-rate test. An analogous plot for constant-head tests is presented in Figure 2-2 on p. 13 in Geier et al. (1996).

2 Investigation methods, interpretation methods and primary data

2.1 Investigation methods

2.1.1 PFL

The Posiva Flow Log (PFL) is a geophysical logging device developed to detect continuously flowing fractures in sparsely fractured crystalline bedrock by means of difference flow logging, see Figure 2-1. The physical limitations of the measurement device and the principles for operation are explained in detail in SKB P-report series, see e.g. Rouhiainen and Sokolnicki (2005).

The flowing fractures detected with the PFL method represent a system subjected to several days of pumping, where the entire borehole acts as a line sink. The device is designed to detect individual fracture flows along the borehole with a high spatial resolution. A resolution of 0.1 m is used in Forsmark. The detection limit varies depending on the in-situ conditions in the borehole, e.g. gas bubbles. As a rule of thumb, the lower detection limit of the flow meter device used is c 30 mL/h.

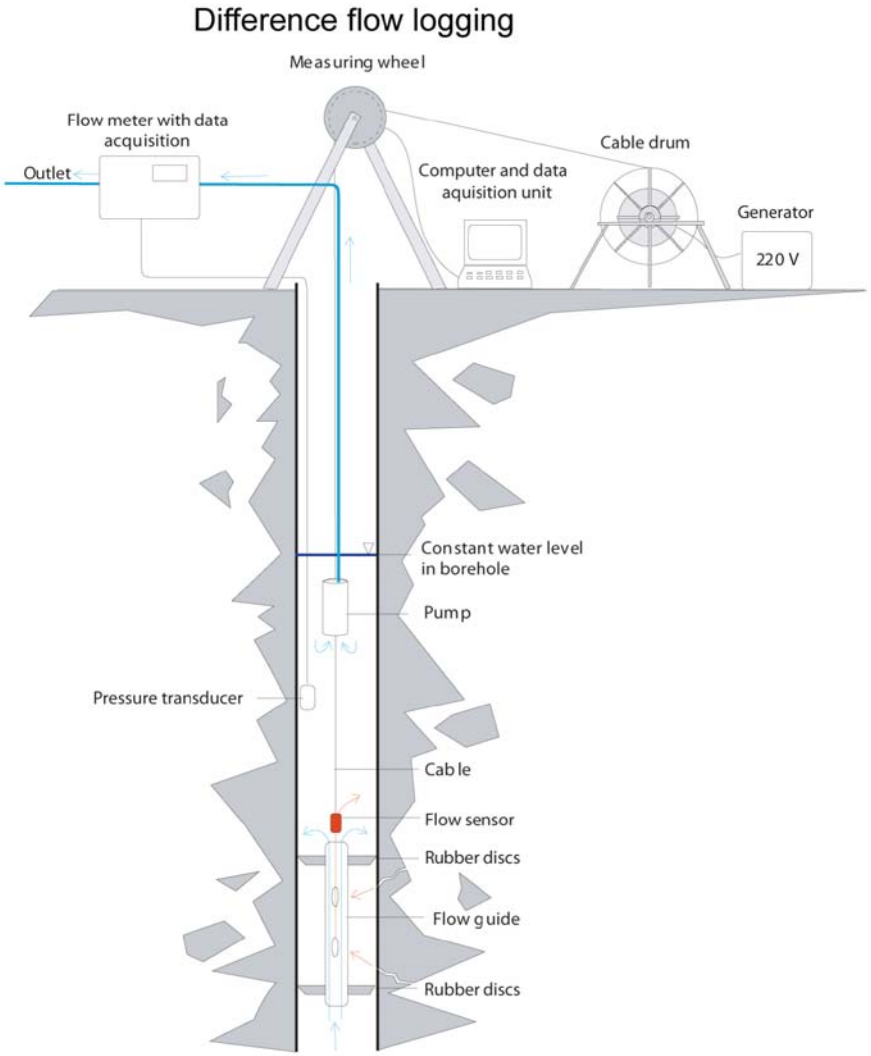

Figure 2-1. *Schematic drawing of the down-hole equipment used for difference flow logging. Reproduced from SKB MD 322.010.*

The PFL method has the following characteristics:

- A radial, steady-state flow regime is assumed to prevail around each test interval. The length of the test interval is probably small enough to characterise the flow from individual fractures. By combining the PFL method with a borehole image viewer, the orientation of the flowing fracture can be assessed. The maximum uncertainty in position along the borehole of the PFL method is c +/– 0.2 m (Forssman et al. 2004).
- There are no problems with flowing fractures short circuiting with the borehole above and below the rubber discs since the borehole is a line sink. Problems with the rubber discs may arise however, e.g. when there are large cavities in the borehole diameter or large axial flows in the borehole below the test interval, see Pöllänen and Sokolnicki (2004).
- A nominal value of the lower measurement limit of the PFL fracture transmissivity can be deduced from the lower detection limit of the flow meter device (cf. above) and the standard constant-head change applied during the long-term pumping, $\Delta h = 10$ m, see Section 2.2.1 for details. In reality, the practical lower measurement limit of the PFL method depends on the borehole conditions. At Forsmark, the practical, lower measurement limit of PFL fracture transmissivity is typically $1 \cdot 10^{-9}$ m^2/s for an applied head difference (drawdown) of 10 metres.
- PFL fracture transmissivity values, T_{PFL}, are only defined and reported to the Sicada data base for those 0.1-m long test intervals where measurable flow rates were observed. Non-flowing test intervals are not assigned a threshold value.

2.1.2 PSS

A schematic drawing of the PSS test equipment used in Forsmark is shown in Figure 2-2. Constant-head injection tests are typically run with three different test section lengths, 100 m, 20 m and 5 m. The length of the injection period of the 5 m tests is 20 minutes, which means that the state of flow during constant-head injection is likely to be more transient than that during difference flow logging. The injection period is followed by a pressure recovery period of the same duration.

The PSS method has the following characteristics:

- The test section is generally so long that several fractures are investigated at the same time. Their individual contribution or geometry cannot be inferred without an additional set of assumptions of statistical nature, e.g. Osnes et al. (1991), Fransson (2002).
- The dominating flow regimes and the state of flow can usually be addressed by analysing the entire injection and recovery periods.
- There may be problems with locally connected fractures short circuiting with the borehole above and below the inflatable packers (cf. Figure 2-2), in particular at locations where the fracture intensity is high close to the test interval.
- A nominal value of the lower measurement limit of the test interval transmissivity can be deduced from the lower detection limit of the flow meter device, which is approximately 60 mL/h, and the standard constant-head change applied during the short-term injection, $\Delta h = 20$ m. Using Moye's transmissivity formula, see Section 2.2.2 for definition, the lower standard detection limit for transmissivity of a 5-m long test interval (section) is c $6.7 \cdot 10^{-10}$ m^2/s.
- Two transmissivity values, one steady-state and one transient, are reported for each PSS test to the Sicada database according to the method description for single-hole hydraulic testing SKB MD 320.004, see Section 2.2.2 for details. The information stored in Sicada is accompanied by a recommendation regarding the transmissivity value of each test interval to be used for groundwater flow modelling. The recommended transmissivity value is here denoted by T_{BC} (BC for "Best Choice").
- If apparent boundary effects can be observed at injection shut-in, this is also reported to the Sicada data base, see Section 2.2.2 for details.

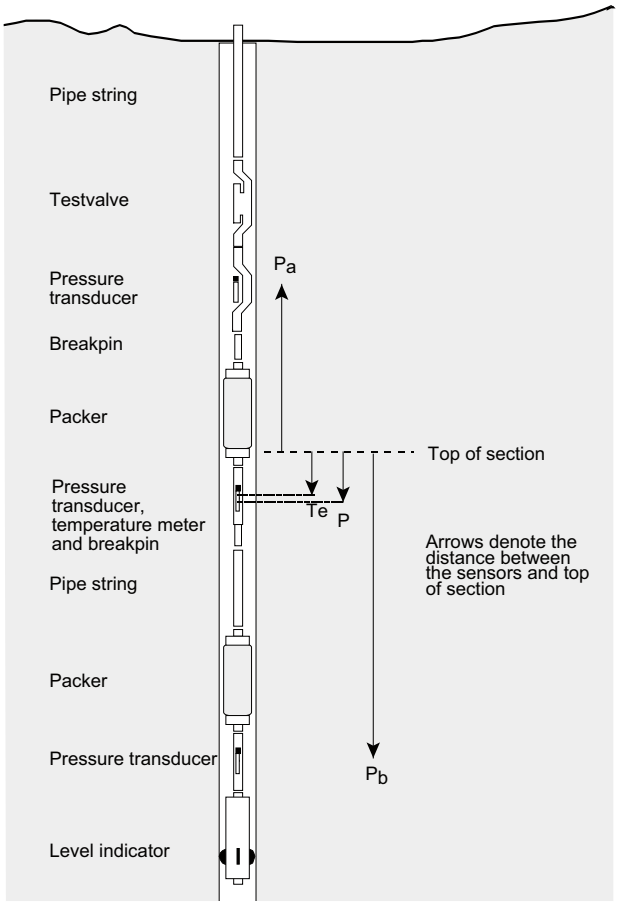

Figure 2-2. *Schematic drawing of the down-hole equipment in the PSS system. Reproduced from SKB MD 323.001.*

2.2 Interpretation methods

2.2.1 Analysis of difference flow logging tests

Ludvigson et al. (2002) present the interpretation procedure used according to the method description SKB MD 322.010 for interpretation of fracture transmissivity using the PFL difference flow logging method. The PFL fracture transmissivity is calculated from Thiem's equation (Thiem 1906) for steady-state radial flow to a well in a finite two-dimensional, homogeneous porous medium:

$$T_{PFL} = (\Delta Q/\Delta h)\,[\ln(r_e/r_w) / (2\pi)] \qquad (2\text{-}1)$$

where T_{PFL} is the steady-state PFL fracture transmissivity (m^2/s), ΔQ is the difference in flow rate (m^3/s), Δh (m) is the difference in head, r_e (m) is the radius of influence and r_w (m) is the nominal value of the borehole radius. The results from the PFL measurements reported to Sicada are based on the assumption that the ratio of r_e/r_w is constant along the borehole, $r_e/r_w = 500$, i.e., with r_w = 0.038 m r_e is 19 m. The ratio value implies that:

$$T_{PFL} \approx \Delta Q/\Delta h \qquad (2\text{-}2)$$

In other words, the values reported to the Sicada database are not fracture transmissivities of the intersecting fractures, but simply the test interval specific capacity of each test interval. As the actual flow geometries, skin effects, and radii of influence are unknown, the transmissivity values derived by Equation (2-2) should be taken as indicating orders of magnitude. A discussion of other potential sources for uncertainty in the estimation of transmissivity using the PFL method is presented in Ludvigson et al. (2002).

2.2.2 Analysis of constant-head injection tests

Ludvigson et al. (2007) present the standard interpretation procedure used according to the method description SKB MD 320.004 for interpretation of test interval transmissivity using the PSS constant-head injection method. Separate transient evaluations are made of the injection and recovery periods of each test, see Figure 2-3. In principle, the standard calculation of the PSS test interval transmissivity is based on Theis' classic theory for transient radial flow to well in an infinite two-dimensional, homogeneous porous medium (Theis 1935, Jacob and Lohman 1952). The transient PSS transmissivity, T_T (m^2/s), is evaluated for different borehole and aquifer conditions by means of type curves using AQTESOLV.

The transient analysis consists of two parts, a diagnostic analysis followed by parameter estimation. The transient analysis of the tests is supplemented by a steady-state analysis of test interval transmissivity. The different test phases are numbered 1–7 and may be explained as follows:

1 = measurement of the open borehole pressure,
2 = start of packer inflation,
3 = shut-in of test section,
4 = start of injection period,
5 = stop of injection period,
6 = stop of pressure recovery,
7 = packer deflation.

Diagnostic analysis

Diagnostic analysis of flow regimes during the test is performed, e.g. wellbore storage (WBS), pseudo-linear flow (PLF), pseudo-radial flow (PRF) and pseudo-spherical flow regime (PSF), respectively, see Figure 2-4. During some tests transitions between different flow regimes occur. In addition, indications of outer boundary conditions, i.e., apparent no-flow boundaries (NFB) or constant-head boundaries (CHB), during the tests are identified. In constant-head tests, effects of wellbore storage are assumed to be negligible during the injection period since pressure is constant.

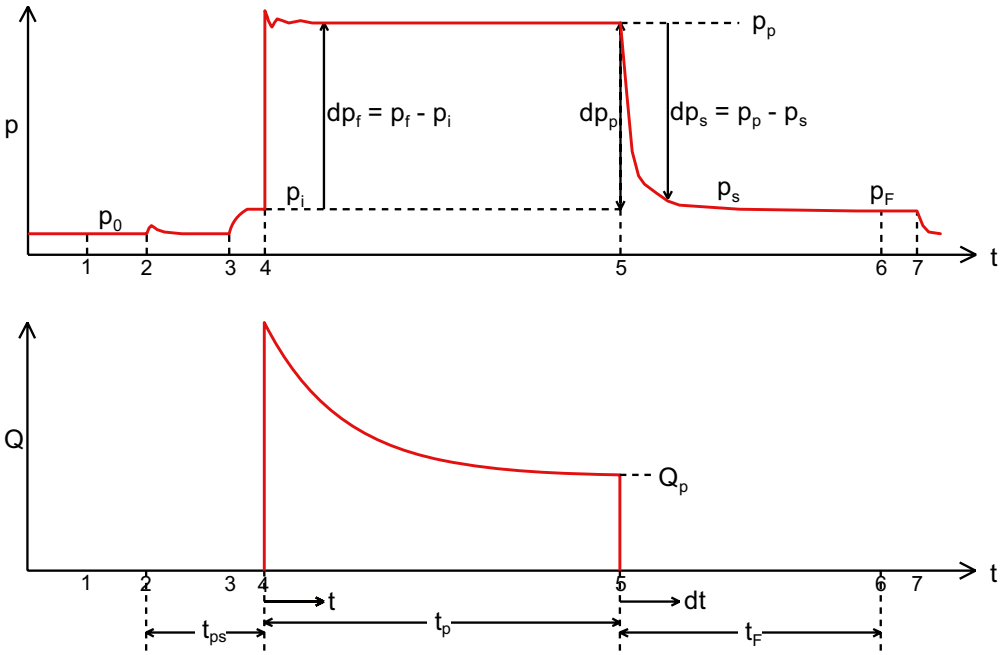

Figure 2-3. *Illustration showing the variation in time (t) of test interval borehole pressure (p) and flow rate (Q) during a constant-head injection test. The numbers represent different test phases and are explained in the text. Reproduced from SKB MD 320.004.*

The diagnostic analysis during the injection period is mainly performed from log-log plots of the inverse of the flow rate for a constant drawdown (dh/Q) together with the corresponding derivative plot. The derivative is calculated using various algorithms and filter factors to achieve appropriate smoothing of the data. The recovery period of the tests is analysed in a corresponding manner, see Ludvigson et al. (2007) for details.

According to SKB MD 320.004, flow regimes may be described in terms of a generalised radius of influence from the borehole, cf. Figure 2-4:

- **Inner zone (iz).** Representing very early response which reflects the hydraulic interaction between the borehole and rock close to the borehole. It may be deteriorated by turbulent head losses or other head losses (drilling debris) or improved by fractures intersecting the borehole. The hydraulic properties of the inner zone are generally expressed in terms of skin factor and WBS (for the recovery period).
- **Middle zone (mz**). Representing the first response from which it is considered possible to evaluate representative hydraulic properties of the rock or hydraulic feature near the borehole, in the time span from t_1 to t_2.
- **Outer zone (oz).** Representing the response of hydraulic feature(s)/boundary conditions connected to the actual hydraulic feature interpreted from the middle zone, at times later than t_2. Sometimes it is possible to deduce the possible character of the hydraulic feature or boundary and sometimes possible to evaluate the hydraulic properties or boundary conditions.

In particular, time intervals with pseudo-radial flow, reflected by a constant (horizontal) derivative in log-log diagrams, are identified. Pseudo-linear flow, indicating flow in a single hydraulic feature, is reflected by a straight line of slope 0.5 (1:2) or less at the beginning of the test, both for the inversed flow rate and its derivative. In many cases, pseudo-linear flow is transitioning to pseudo-radial during the test, see Figure 2-4. A true spherical flow regime (3D) is reflected by a straight line with a slope of –0.5 for the derivative. Steeper slopes of the derivative may indicate transitions to pseudo-spherical (leaky) or ultimately, pseudo-stationary flow caused by apparent constant-head boundaries, reflected by almost steady-state conditions with a rapidly decreasing derivative. Pseudo-spherical flow, as defined here, may be conceptually interpreted in several ways, for example an increasing cross-sectional flow area with distance away from the borehole (e.g. flow in a thick, well-connected fracture zone), or an increasing transmissivity with distance away from the borehole (e.g. due to interconnecting fractures with higher transmissivity at some distance).

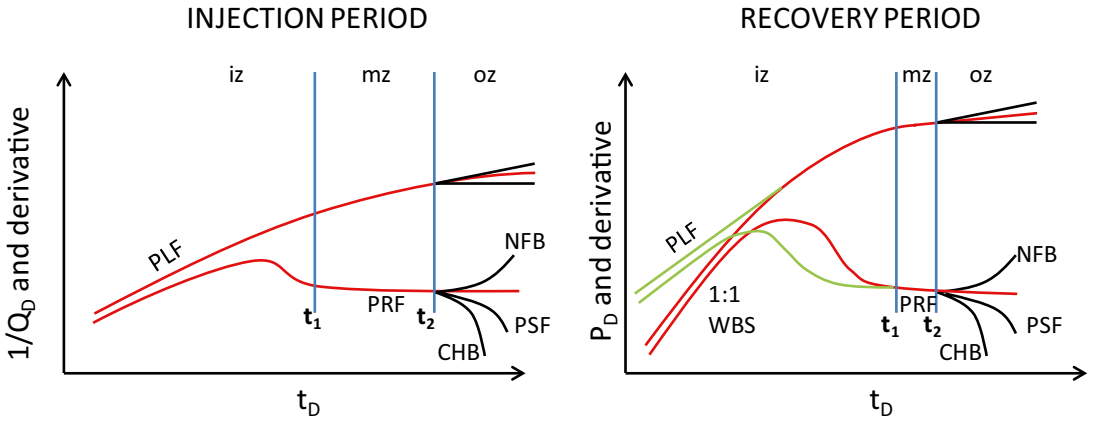

Figure 2-4. Schematic log-log plots of transient test responses and associated derivatives during the injection period and the recovery period of a constant-head injection test. The notation and symbols are explained in the text.

Transient analysis

For the injection period, the modification by Hurst et al. (1969) of the standard theoretical model for constant-head tests in porous media by Jacob and Lohman (1952) is applied for estimating the transmissivity and skin factor when a certain period with pseudo-radial flow could be identified from the data curve. If more than one interval with pseudo radial flow is identified, the representative parameter estimation should be made on the earliest interval and reported in the Sicada data base according to SKB MD 320.004.

For tests showing apparent pseudo-spherical (leaky) flow, eventually transitioning to pseudo-stationary flow during the injection period, a model by Hantush (1959) for radial to leaky flow during constant-head tests is used for the evaluation. For tests exhibiting fracture flow responses (a straight line of slope 0.5 or less in a log-log plot), eventually transitioning to pseudo-radial flow regime, the standard radial flow model by Hurst et al. (1969) in combination with a strongly negative skin factor is generally used as this behaviour is almost identical to that of a fracture flow model. In addition to the model by Hurst et al. (1969), special models for single fractures are in some cases also used as a complement to the standard radial-flow models described above.

The transient analysis of the tests is made using AQTESOLV with the models described above. The transmissivity and skin factor are calculated from the type curve matching assuming a fixed value on storativity. The storativity was calculated using an empirical relationship in Equation (2-3) derived from hydraulic interference tests at Äspö HRL, see Rhén et al. (1997):

$$S = 7 \cdot 10^{-4} \cdot T^{0.5} \qquad (2\text{-}3)$$

S = storativity (–)

T = transmissivity (m^2/s)

The recovery period of the constant-head tests is analysed in an analogous manner, see Ludvigson et al. (2007).

Steady-state analysis

A preliminary steady-state analysis of transmissivity, T_M (m^2/s), according to Moye's formula (Moye 1967) is made for the flow rate at the end of the injection period using the following equation (cf. Figure 2-3):

$$T_M = [(Q_p \rho_w g) / dp_p] C_M \qquad (2\text{-}4)$$

$$C_M = [1 + \ln(L/(2r_w))] / 2\pi \qquad (2\text{-}5)$$

Q_p = flow rate by the end of the flow period (m^3/s)

ρ_w = density of water (kg/m^3)

g = acceleration of gravity (m/s^2)

C_M = geometrical shape factor (–)

dp_p = final injection pressure, $dp_p = p_p - p_i$ (Pa)

r_w = borehole radius (m)

L = test interval length (m)

Moye's formula is similar to the Theim's equation with the addition of a "shape" factor that assumes the rock is a homogeneous, porous continuum such that the flow is radial at the centre of the test section and becomes spherical at the ends. Some of its effects appear in Figure 1-4. There is no practical way to determine whether Moye or Theim is more appropriate, however, it does not make a difference in the transmissivity results in practice.

Representative transmissivity and best choice transmissivity

According to the method description SKB MD 320.004, a representative transient transmissivity, T_T, either from the injection period or the recovery period of each test, is evaluated. In most cases, this transmissivity is selected from the injection period. Secondly, a best-choice transmissivity, T_{BC},

for each test is selected. For tests where transient evaluation was not possible, or ambiguous, the steady-state transmissivity, T_M, was selected as T_{BC}. For example, T_M is chosen if a pseudo-linear flow regime (PLF) occur at all times during both test periods (a straight line in a log-log plot).

Estimation of the radius of influence

According to the method description SKB MD 320.004, a rough estimation of the equivalent radius of influence (r_i) of each PSS test is made from the identified (earliest) radial-acting flow period based on the inferred representative transmissivity (T_T) and storativity (S) from Equation (2-6):

$$r_i = (2.25\ T_T\ t\ /S)^{½} \qquad (2\text{-}6)$$

r_i = radius of influence of the first radial-acting flow period (m)

t = elapsed time at the end of the first radial-acting flow period (s)

T_T = representative transmissivity of the first radial-acting flow period (m^2/s)

S = storage coefficient, see Equation (2-3)

Equation (2-6) is shown in Figure 2-5.

In addition, an r_i-index (–1, 0 or +1) is defined to characterise the hydraulic response by the end of each injection test. It is assumed that a certain time interval with pseudo-radial flow (PRF) can be identified between t_1 and t_2 during the test, see Figure 2-4. The r_i-index is defined as:

- r_i-index = 0: The transient response indicates that the size of the hydraulic feature tested is greater than the radius of influence based on the actual test time ($t_2 = t_p$), i.e. the PRF is continuing at stop of the test. This fact is reflected by a flat derivative at this time.
- r_i-index = +1: The transient response indicates that the hydraulic feature tested is connected to a hydraulic feature with lower transmissivity or an apparent barrier boundary (NFB). This fact is reflected by an increase (+ slope) of the derivative. The size of the hydraulic feature tested is estimated as the radius of influence based on t_2.
- r_i-index = –1: The transient response indicates that the hydraulic feature tested is connected to a hydraulic feature with higher transmissivity or an apparent constant-head boundary (CHB). This fact is reflected by a decrease (– slope) of the derivative. The size of the hydraulic feature tested is estimated as the radius of influence based on t_2.

If a certain time interval of PRF cannot be identified during the test, the r_i-indices +1 and –1 are still defined as above and the radius of influence according to Equation (2-6) is estimated using the actual flow time t_p shown in Figure 2-3 together with T_M.

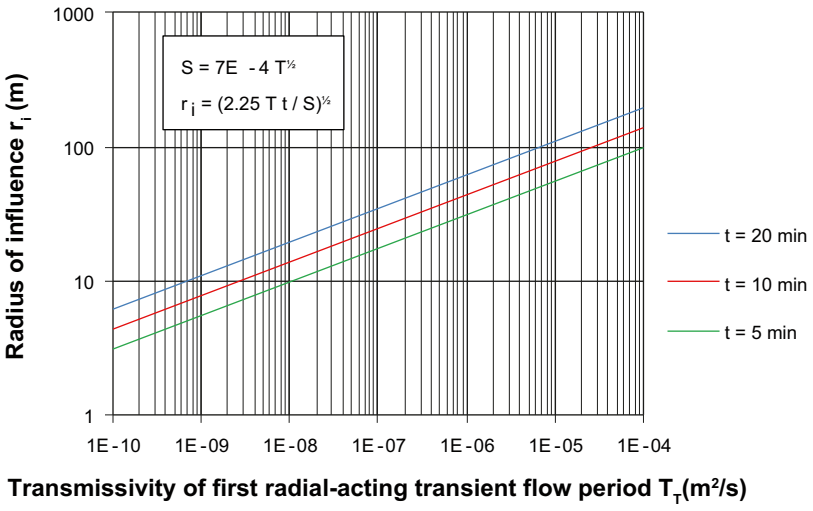

Figure 2-5. *Plot of the radius of influence versus the transmissivity T_T and duration t of the first-radial acting transient flow period.*

2.2.3 GRF analysis of constant-head injection tests

Theory

The GRF model presented by Barker (1988) is based on a generalised description of how the flow cross-sectional area changes with distance in an n-dimensional space. The basic equation for a unit cross-sectional area in n dimensions is:

$$A = \alpha_n \, r^{n-1} \qquad (2\text{-}7)$$

where

$$\alpha_n = (2\pi^{n/2}) / \Gamma(n/2) \qquad (2\text{-}8)$$

and $\Gamma(x)$ is the gamma function.

For integer flow dimensions:

n = 1 $A = 2$ (surface area of a square of unit side)

n = 2 $A = 2 \pi r$ (surface area of a cylinder of unit height)

n = 3 $A = 4 \pi r^2$ (surface area of a sphere)

Equation (2-7) is valid for a unit volume. The actual volume also depends on a factor b, which is described as the extent of the flow zone. The interpretation of b for integer dimensions is simple: for n = 1, b is the side of a square so that A becomes $2b^2$; for n = 2, b is the height of the cylinder so that A becomes $2\pi rb$; for n = 3, b has no physical meaning. Generally, the surface area of an n-dimensional space, including the factor b, is:

$$A = b^{3-n} \, \alpha_n \, r^{n-1} \qquad (2\text{-}9)$$

The analysis of constant-head tests according to the GRF concept was presented by Doe and Geier (1990) and applied to constant-head tests in Sweden by Geier et al. (1992, 1996). For an integer dimension of two, b is the familiar thickness of the aquifer, fracture zone, test interval length, etc, and r is the radius away from the borehole. Under such conditions, the transmissivity T may be estimated as the product T = Kb. However, the meaning of b and r become more difficult at other flow dimensions.

According to Doe and Geier (1990), the dimensionless flow rate Q_D and dimensionless time t_D in the GRF concept are both functions of the hydraulic conductivity of the flowing conductor, K_c (m/s). In the case no borehole skin factor, S_w (–), the effective radius of the borehole (Earlougher 1977) is the same as the nominal radius of the borehole r_w (m) and Q_D and t_D may be written as:

$$Q_D = Q / [dh \, K_c \, b^{3-n} \, \alpha_n \, r_w^{n-2}] \qquad (2\text{-}10)$$

$$t_D = (K_c \, t) / (S_s \, r_w^2) \qquad (2\text{-}11)$$

Geier et al. (1996) noted that in fractured rock, frequently a single fracture or channel is responsible for virtually all of the flow. In such a case, the estimate of K_c will be misleading as a description of the conduit's hydraulic conductivity, since it is a function of the test interval length, L (m), which has nothing or little to do with the conducting thickness of the primary conduit, b (m). If the ratio of the conducting thickness to the test interval length is known, b/L (–), a more meaningful value of K_c may be obtained by dividing by this ratio. However, in general the conducting thickness is not known within an order-of-magnitude accuracy. Geier et al. (1996) did not evaluate K_c in their type curve analyses of PSS constant-head injection tests conducted in boreholes KAS02–KAS08 at the Äspö HRL, but defined a generalised transmissivity T_{GRF} (m^2/s):

$$T_{GRF} = (K_c \, b^{3-n} \, r_w^{n-2}) \qquad (2\text{-}12)$$

which is independent of test interval length L. In case of cylindrical flow, this is the classic two-dimensional flow transmissivity. For dimension 1 this reduces to Kb^2/r_w. For dimension 2 it is Kb. For dimension 3, it is $K \, r_w$. Also the transmissivity calculation depends on the alpha, which is 2π for dimension 2.

This work

The GRF analysis implemented in AQTESOLV is based on the theory of Barker (1988) and involves six parameters for the interpretation of the injection period of a PSS test:

- hydraulic conductivity, K_{GRF} (m/s)
- specific storativity, $S_{s,GRF}$ (m^{-1})
- flow dimension, n_{GRF} (–)
- extent of the flow zone, b (m)
- skin factor, S_w (–)
- borehole radius, r_w (m)

During the type curve matching in AQTESOLV, three parameters are estimated, n_{GRF}, K_{GRF}, and S_w, for predefined values of S_s, b, and r_w. The simplification made in AQTESOLV concerns the parameter b, which was assumed to be equal to the test interval length, i.e., b = L regardless of the flow dimension n_{GRF}. Hence, the generalised transmissivity value of T_{GRF} in AQTESOLV is calculated as:

$$T_{GRF} = K_{GRF}\, L \qquad (2\text{-}13)$$

As for Equation (2-12), the transmissivity deduced from the GRF analysis in AQTESOLV is the classic two-dimensional flow transmissivity for cylindrical flow.

The flow dimension derived from the GRF analysis using AQTESOLV is here designated by n_{GRF}. Furthermore, it is noted that the GRF concept in AQTESOLV is restricted to fractional flow dimensions in the interval 0–3.

2.3 Primary hydraulic data

A number of PSS injection tests from boreholes KFM02A, KFM03A and KFM06A are selected for GRF analysis to compare with the standard PSS analysis reported in Källgården et al. (2004), Hjerne et al. (2005), and Svensson et al. (2005), respectively. The results are also compared with the results from difference flow logging using the PFL method in the corresponding boreholes reported by Pöllänen and Sokolnicki (2004), Rouhiainen and Pöllänen (2004), and Rouhiainen and Sokolnicki (2005), respectively.

The primary hydraulic data, i.e., PSS and PFL data, reported to the Sicada data base from the three boreholes are shown in Appendix A together with the geological interpretations. Only 5-m long test intervals above the test-specific lower measurement limit of the PSS method are analysed in the work reported here. Hence, in all the analysed test intervals both injection tests with the PSS method and difference flow loggings with the PFL method are performed. In this study, the results from the fracture-specific PFL measurements are used (PFL-f). The PFL fracture transmissivities in each 5-m interval are added together to form an integrated PFL transmissivity value of this interval.

All boreholes are located in the main rock domain inside the tectonic lens at Forsmark (RFM21). With reference to Figure 1-1 the following geological conditions are noted:

- Borehole KFM06A is located in the footwall of the gently dipping deformation zones ZFMA2. In this borehole we analyse 58 PSS tests with the simplified GRF method.
- Borehole KFM02A intersects ZFMA2 at about –440 m of elevation. In this borehole we analyse 45 PSS tests with the simplified GRF method.
- Borehole KFM03A is located in the hanging wall of ZFMA2. In this borehole we analyse 48 PSS tests with the simplified GRF method.

3 Results

3.1 Introduction

To demonstrate what is meant by standard analysis and GRF analysis of constant-head injection tests in 5-m long test intervals, four selected examples are shown in Figures C-1 to Figure C-4 in Appendix C. The four examples illustrate the identification of standard flow regimes and estimated GRF flow dimensions using AQTESOLV. The parameter designations in these plots are explained in Chapter 2 and Table 3-1. Table B-1 summarises the derived parameter values of the four test intervals including the corresponding difference flow logging transmissivities using the PFL method.

3.2 Assignment of flow dimension codes

In order to compare the interpreted dominating flow regimes (PLF, PRF, PSF and NFB) from the standard analysis of Ludvigson et al. (2007) with the flow dimensions estimated from the GRF analysis, the former are assigned flow dimension codes according to Table 3-1. The identification of flow regimes using standard analysis is described in Section 2.2.2.

Table 3-1. Analysed number of PSS tests in boreholes KFM02A, KFM03A and KFM06A grouped by flow regime (PLF, PRF, PSF and NFB). Each group is assigned a flow dimension code to allow for comparisons with the estimated flow dimensions from the GRF analysis. Tests with more than one characteristic flow regime are denoted by an arrow, e.g. PLF→PRF.

Dominating flow regime of the test	Flow dimension code	Number of tests in each flow regime		
		KFM02A	KFM03A	KFM06A
NFB[4]	0.5	0	0	6
PLF[1]	1	0	1	3
PLF→ PRF	1.5	1	0	3
PRF→NFB	1.5	6	9	11
PRF[2]	2	27	26	23
PRF→PSF	2.5	7	7	5
PSF→NFB	2.5	1	0	1
PSF[3]	3	3	5	6
Number of PSS tests		**45**	**48**	**58**

[1] PLF = pseudo-linear flow.
[2] PRF = pseudo-radial flow.
[3] PSF = pseudo-spherical flow.
[4] NFB = apparent no-flow boundary.

- Tests assigned a code =1 (PLF) exhibit a dominating pseudo-linear flow regime during the injection period (often characterised by a straight line in a log-log diagram). Such tests are often reflected by a strong negative skin factor. An example of such a test is shown in Figure C-1a in Appendix C.
- Tests assigned a code =2 (PRF) exhibit a dominating pseudo-radial flow regime (characterised by a horizontal derivative in a log-log diagram). An example of such a test is shown in Figure C-2a in Appendix C.
- Tests assigned a code =3 (PSF) show a dominating pseudo-spherical flow regime during the injection period. However, tests with idealised spherical flow are rather uncommon. Therefore, most tests with a code of 3 correspond to pseudo-spherical (leaky) flow, eventually approaching steady-state flow if an apparent constant-head boundary is encountered. An example of a test with pseudo-spherical flow is shown in Figure C-3a in Appendix C.

Tests showing transitions of flow regimes are coded between the Euclidian flow regimes, e.g. 1.5. Two kinds of transitions of flow regimes are coded as 1.5. The first case is when a certain period of pseudo-linear flow is transitioning to pseudo-radial flow (PLF→PRF). The second case is when a period of pseudo-radial flow is transitioning into an apparent no-flow boundary (PRF→NFB).

An apparent NFB is here defined as a rapid increase of the inverse of the flow derivative in contrast to the classic definition of a no-flow boundary in porous media, which mostly refers to a linear boundary. Thus, an apparent NFB may correspond to any kind of flow restriction. If the test time is long enough, a second period with pseudo-radial flow may develop, reflecting hydraulic contact with a second hydraulic unit of lower transmissivity (composite system, cf. Geier et al. (1996)).

Tests coded with a flow regime of 2.5 also involve two kinds of transitions. The first case is when a period of pseudo-radial flow is transitioning to pseudo-spherical flow (PRF→PSF). The second case is when a period of pseudo-spherical flow is transitioning to an apparent no-flow boundary (PSF→NFB). An apparent NFB is defined as explained above.

Finally, during some tests no well-defined flow regime develops during the test. Tests with a dominating apparent no-flow boundary (i.e., a strongly decreasing flow rate) during most of the injection period are denoted as NFB with a code of 0.5. Such tests may sometimes start with a short period of another apparent flow regime, e.g. PRF, which might indicate a fracture of limited extension intersecting the test interval, alternatively a decreasing fracture aperture. An example of such a test is shown in Figure C-4a in Appendix C. For such tests, an unambiguous transient analysis can often not be done of the injection period. Instead, transient analysis is made of the pressure recovery period of the tests.

Some tests may also show a dominating, apparent positive hydraulic boundary (CHB) during the injection period, indicating a flow dimension greater than 3. The first part of the injection period may be distorted due to oscillating pressure during the stabilisation time to a constant pressure in the test section. This fact may lead to that the initial flow regime during the test is masked (e.g. PLF) and thus under-represented in the inferred flow regimes.

3.3 GRF flow dimension intervals

The results from the GRF analysis of the four selected examples constant-head inject tests are shown in Figure C-1b through Figure C-4b in Appendix C.

The interpreted flow dimensions (n_{GRF}) of the selected injection tests in boreholes KFM02A, KFM03A and KFM06A using AQTESOLV are aggregated into intervals according to Table 3-2 below. The middle value of each interval is selected to be directly comparable with the assignment of flow dimension codes, see Section 3.2.

Table 3-2. Analysed number of PSS tests in boreholes KFM02A, KFM03A and KFM06A grouped by GRF flow dimension intervals.

Flow dimension code (Table 3-1)	GRF flow dimension intervals	Number of tests in each GRF class		
		KFM02A	KFM03A	KFM06A
0.5	<0.75	1	0	8
1	0.75–1.25	2	0	2
1.5	1.25–1.75	5	10	13
2	1.75–2.25	19	12	18
2.5	2.25–2.75	5	9	5
3	2.75–3.25	13	17	12
Number of PSS tests		**45**	**48**	**58**

3.4 Standard analysis versus GRF analysis in KFM06A

The estimated flow dimensions from standard analysis and GRF analysis, respectively, of the selected tests in KFM06A are cross-plotted in Figure 3-1. The two analysis methods give consistent results. It should be noted that the GRF concept implemented in AQTESOLV is restricted to $n_{GRF} \leq 3$.

Figure 3-2 shows the distributions of estimated flow dimensions from standard analysis and GRF analysis in KFM06A. Both analysis methods show that a flow dimension of 2±0.25 (pseudo-radial flow) is dominating in KFM06A. It is also noted that tests with a flow dimension of less than 0.75 (apparent no-flow boundaries) are relatively common in this borehole.

The cumulative distribution of the estimated flow dimensions from the GRF analysis of the tests in KFM06A is shown in Figure 3-3. The figure shows that the median value of n_{GRF} of the 58 tests is close to two which corresponds to an ideal radial flow regime. The tests with a flow dimension of less than 0.75 show a significant spread.

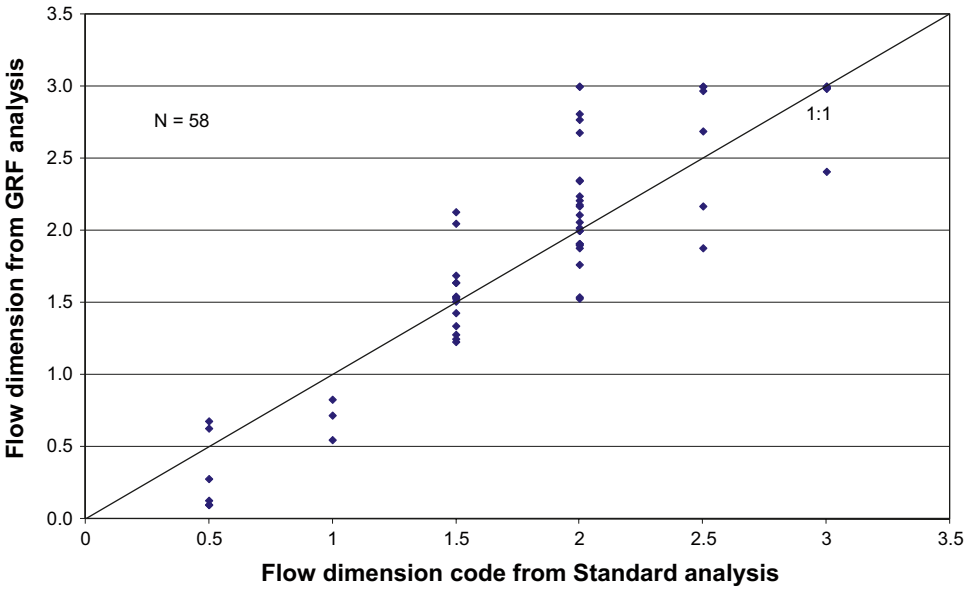

Figure 3-1. Comparison of estimated flow dimensions from standard analysis and GRF analysis of 58 constant-head injection tests in KFM06A.

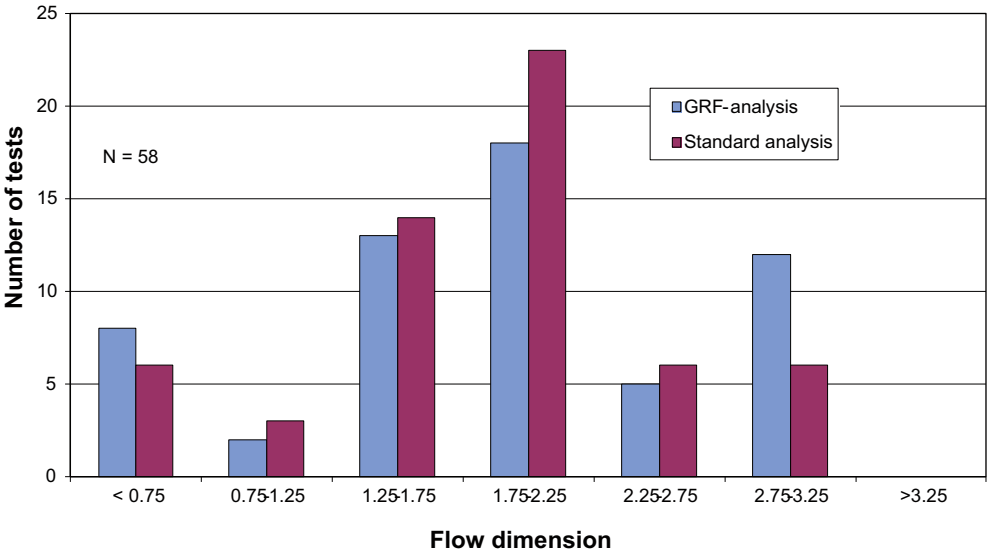

Figure 3-2. Distribution of estimated flow dimensions from standard analysis and GRF analysis of 58 constant-head injection tests in KFM06A.

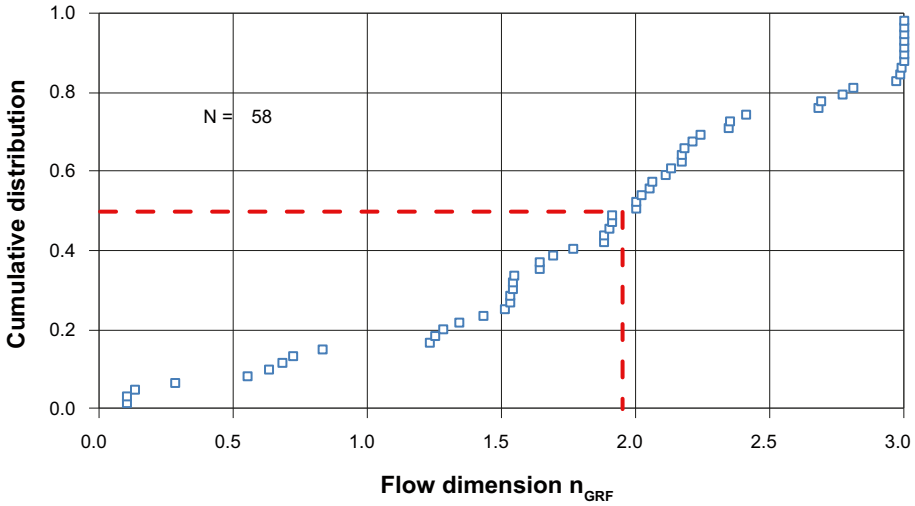

Figure 3-3. *Cumulative distribution of the estimated flow dimensions from GRF analysis of 58 constant-head injection tests in KFM06A.*

Figure 3-4 shows a cross-plot of estimated transmissivities from GRF analysis (T_{GRF}) versus the best-choice transmissivities from the standard analysis (T_{BC}). The plot indicates a good agreement between T_{GRF} and T_{BC} except for a few cases where the estimated T_{GRF} values are much greater (filled squares). Adjacent to the filled squares, the upper position of each test interval (Secup) and the estimated flow dimension from the GRF analysis are shown. A common feature of these test intervals is that the flow dimensions are quite low. As discussed above, the evaluation of the T_{GRF} is considerably more uncertain than the estimation of n_{GRF}. Besides the flow dimension, T_{GRF} is also affected by the assumed value of the extent of the flow zone parameter b.

Figure 3-5 shows a scatter plot of the estimated GRF flow dimensions from the injection period of the PSS tests versus the observed final pressure recovery (fraction) at the end of the recovery period in borehole KFM06A. The final pressure recovery is calculated as the fraction of the final pressure recovery at the end of the recovery period (p_p-p_F in Figure 2-3) in relation to the applied injection head (p_p-p_i). The figure shows that the final pressure recoveries for the filled squares in most cases are low, which again suggest poorly connected fracture network geometries for the associated test sections, i.e., compartmentalised fracture networks or hydraulic chokes. A pressure recovery greater than 1 simply indicates that the initial pressure was not fully stabilised before the test started, i.e., it was decreasing.

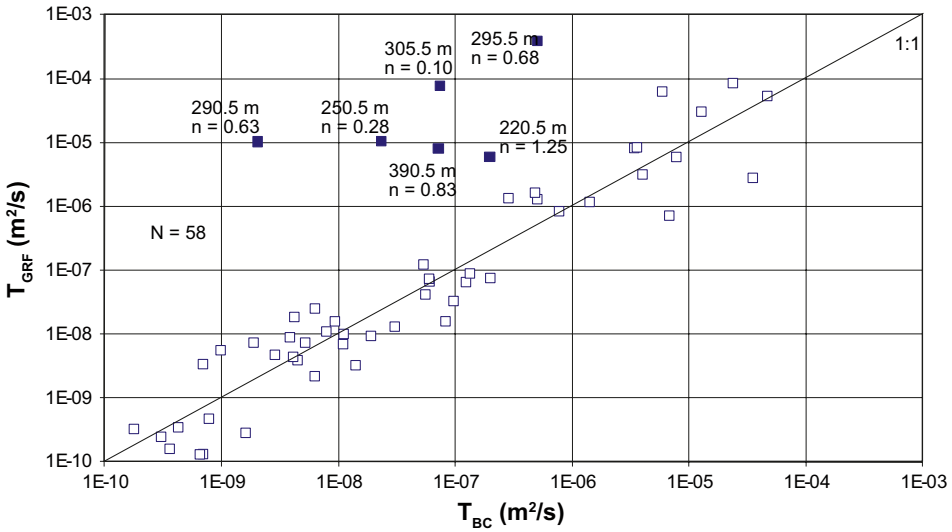

Figure 3-4. *Cross-plot of estimated transmissivities from GRF analysis (T_{GRF}) versus the best-choice transmissivities (T_{BC}) from the standard analysis in KFM06A.*

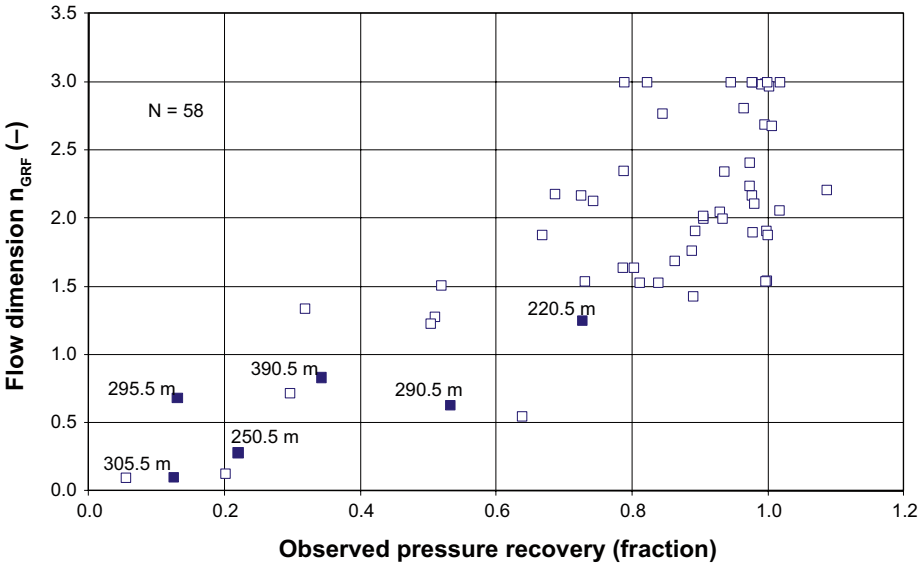

Figure 3-5. *Scatter plot of estimated flow dimensions from GRF analysis (n_{GRF}) versus the observed pressure recovery (fraction) for the same tests as in the previous figure in KFM06A.*

Figure 3-6 shows a cross-plot of the sum of estimated PFL fracture transmissivities in the 58 intervals in KFM06A versus the best-choice transmissivities (T_{BC}) from the standard analysis of the corresponding constant-head injection tests. Test intervals without flowing fractures according to the PFL method are in Figure 3-6 plotted at an arbitrary low value of the transmissivity on the ordinate axis.

Figure 3-6 shows a general good agreement between the estimated transmissivities from the types of test methods. However, for the marked sections with low GRF flow dimensions, the estimated T_{BC} from the standard analysis are in most cases significantly higher than from corresponding ΣT_{PFL}. In section 290.5–295.5 m, there is no flow recorded above the measurement limit in the difference flow logging, cf. Section 2.1.1. Values of ΣT_{PFL} above the 1:1 slope are probably due to different measurement, interpretation or methodological uncertainties. For instance, there is a risk for double-counting in the calculation of ΣT_{PFL}. This would occur if two or more intersecting fractures within a 5-m test interval merge to a single fracture away from the borehole.

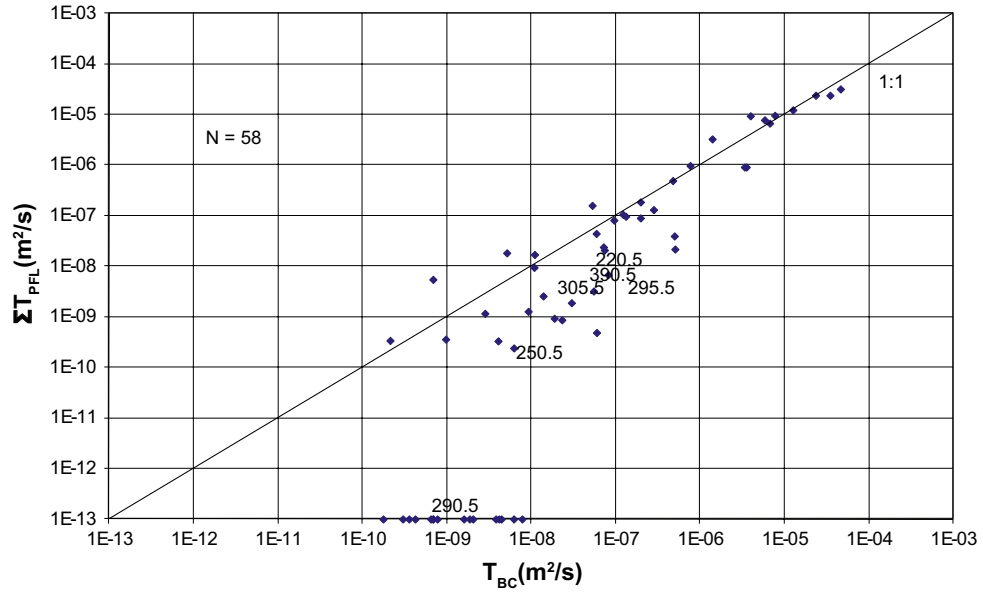

Figure 3-6. *Cross-plot of the sum of PFL fracture transmissivities (ΣT_{PFL}) versus the best-choice transmissivities (T_{BC}) from the standard analysis of 58 constant-head injection tests in KFM06A.*

There are several sections in boreholes KFM01A–KFM07A with T_{BC} less than c $1 \cdot 10^{-8}$ m^2/s for which no conductive fractures could be detected during difference flow logging with the PFL method. In several of these sections the flow rate would probably have decreased below the measurement limit if the injection tests had longer duration. The marked sections with low GRF flow dimensions in Figure 3-4, Figure 3-5, and Figure 3-6 are further discussed in Section 3.7.

3.5 Standard analysis versus GRF analysis in KFM02A

The estimated flow dimensions from standard analysis and GRF analysis respectively of the selected tests in KFM02A are cross-plotted Figure 3-7. The dominating flow regime from the standard analysis is pseudo-radial flow. No tests with (coded) flow regimes lower than 1.5 were interpreted for these tests. It should be recalled that the GRF concept implemented in AQTESOLV is restricted to $n_{GRF} \leq 3$.

In Figure 3-8, the distributions of estimated flow dimensions from standard analysis and GRF analysis in KFM02A are shown. Both analysis methods show that a flow dimension of 2±0.25 (pseudo-radial flow) is dominating. It should be noted that tests with a flow dimension less than 0.75 (apparent no-flow boundaries) are uncommon in this borehole.

The cumulative distribution of the estimated flow dimensions from the GRF analysis of the tests in KFM02A is shown in Figure 3-9. The figure shows that the median value of n_{GRF} of the 45 tests is close to 2, a value that corresponds to an ideal radial flow regime.

Figure 3-10 shows a cross-plot of estimated transmissivities from GRF analysis (T_{GRF}) versus the best-choice transmissivities from the standard analysis (T_{BC}) of the selected constant-head injection tests in KFM02A shown above. The figure indicates a fairly good agreement between T_{GRF} and T_{BC} in most cases in this borehole. This is expected due to the few sections with low flow dimensions, cf. Figure 3-8.

Figure 3-11 shows a scatter plot of the estimated GRF flow dimensions, n_{GRF}, from the injection period of the tests versus the observed pressure recovery (fraction) at the end of the recovery period in borehole KFM02A. The final pressure recovery is calculated as the percentage of the final recovery of the applied injection head in relation to the total injection head at the end of the recovery period. The figure shows that the final pressure recoveries are, in general, close to 1 (complete recovery) in this borehole. The section with a low final recovery corresponds to a low-transmissive section showing effects of apparent no-flow boundaries at the end.

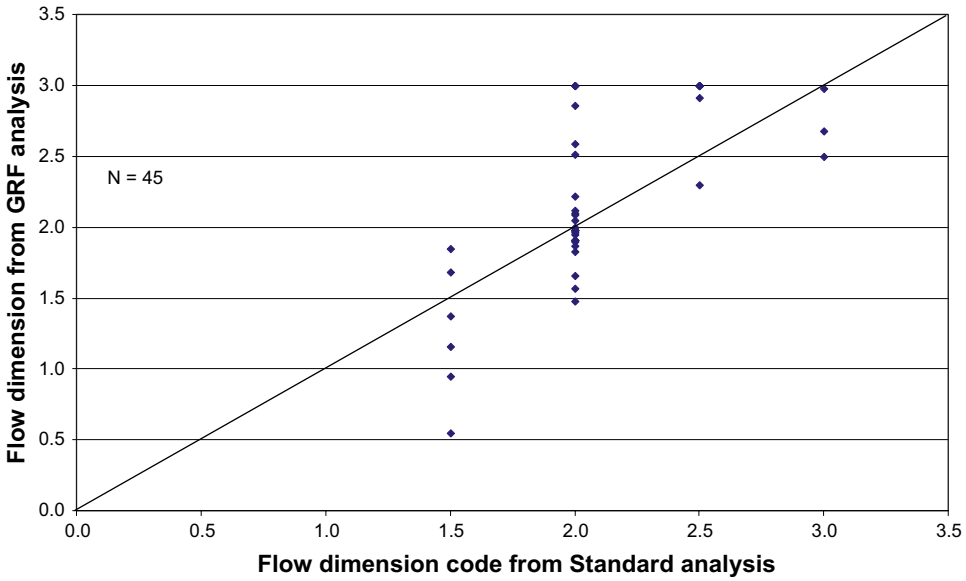

Figure 3-7. *Comparison of estimated flow dimensions from standard analysis and GRF analysis of 45 constant-head injection tests in KFM02A.*

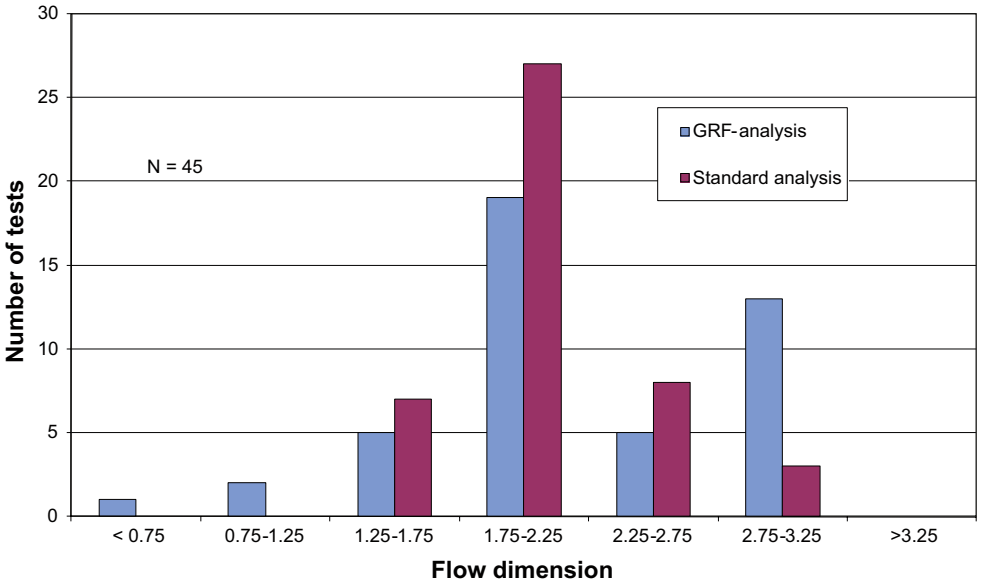

Figure 3-8. *Distribution of estimated flow dimensions from standard analysis and GRF analysis of 45 constant-head injection tests in KFM02A.*

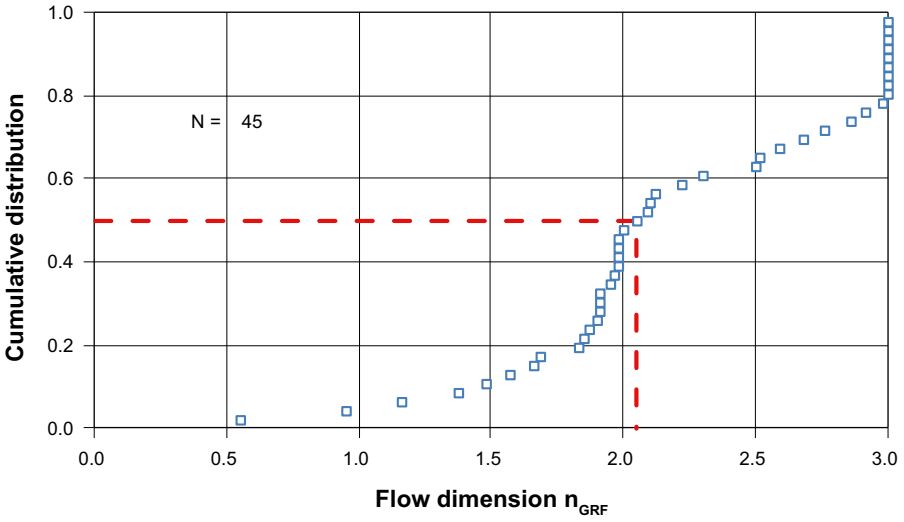

Figure 3-9. *Cumulative distribution of the estimated flow dimensions from GRF analysis of 45 constant-head injection tests in KFM02A.*

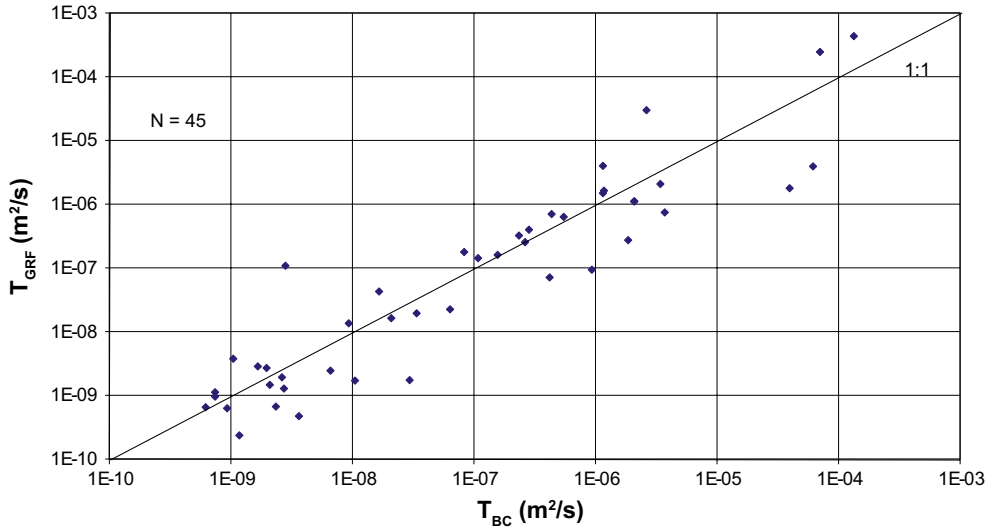

Figure 3-10. *Cross-plot of estimated transmissivities from GRF analysis (T_{GRF}) versus the best-choice transmissivities (T_{BC}) from the standard analysis in KFM02A.*

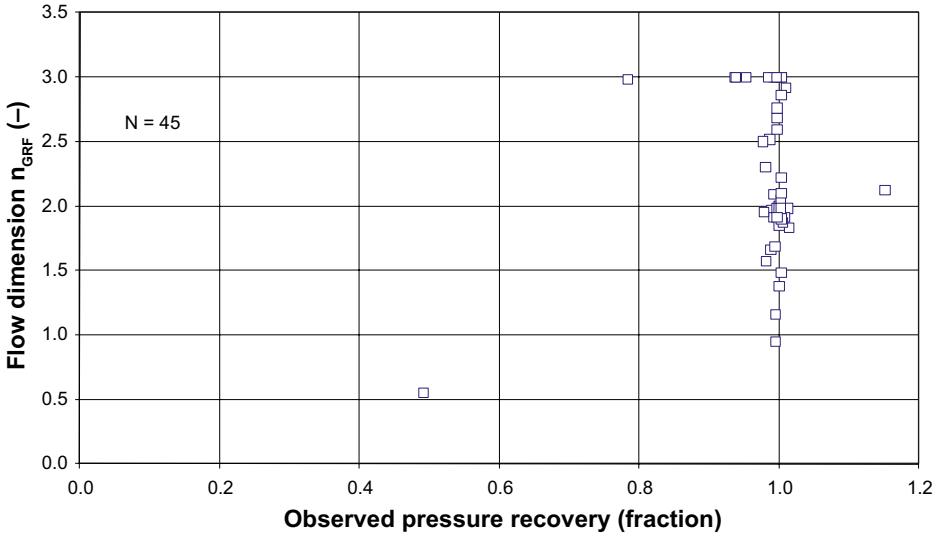

Figure 3-11. *Scatter plot of estimated flow dimensions from GRF analysis (n_{GRF}) versus the observed pressure recovery (fraction) for the same tests as in the previous figure in KFM02A.*

Figure 3-12 shows a cross-plot of the sum of estimated PFL fracture transmissivities (ΣT_{PFL}) versus the best-choice transmissivities (T_{BC}) from the standard analysis of the selected constant-head tests in KFM02A. Sections in which no conductive fractures could be detected in the PFL-fracture measurements are plotted at an arbitrary low value on the ordinate axis. The figure shows general good agreement between the lumped PFL fracture transmissivities and the PSS injection test transmissivities. In some test sections with T_{BC} below c $3 \cdot 10^{-9}$ m^2/s, no conductive fractures could be detected by difference flow logging. The lowest value of the sum of ΣT_{PFL} is c $3 \cdot 10^{-9}$ m^2/s in this borehole. As previously mentioned, values of ΣT_{PFL} above the 1:1 slope are probably due to different measurement, interpretation or methodological uncertainties, e.g. due to double-counting in the calculation of ΣT_{PFL}. This would occur if two or more intersecting fractures within a 5-m test interval merge to a single fracture away from the borehole.

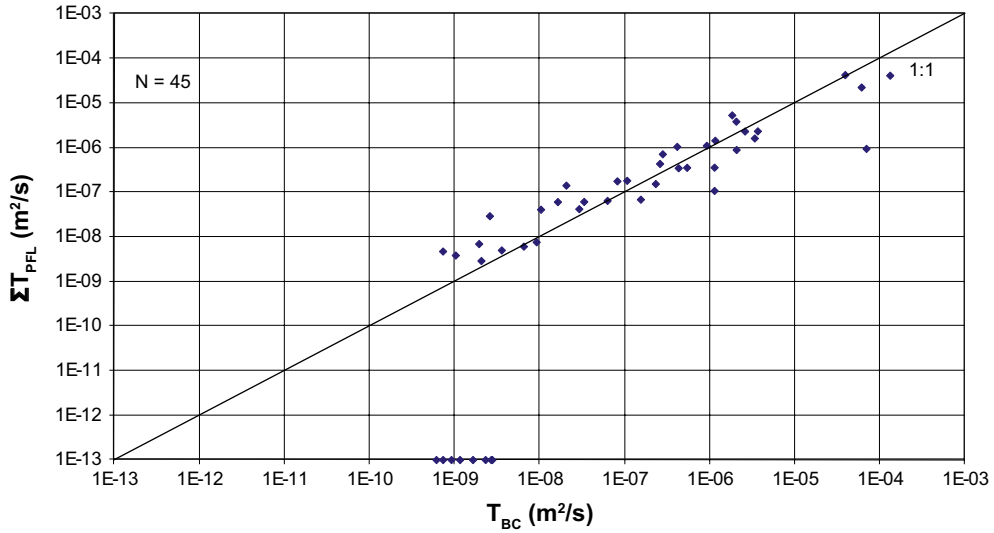

Figure 3-12. *Cross-plot of the sum of PFL fracture transmissivities (ΣT_{PFL}) versus the best-choice transmissivities (T_{BC}) from the standard analysis of 45 constant-head injection tests in KFM02A.*

3.6 Standard analysis versus GRF analysis in KFM03A

The estimated flow dimensions from standard analysis and GRF analysis respectively of the selected tests in KFM03A are cross-plotted in Figure 3-13. The dominating flow regime from the standard analysis is pseudo-radial to pseudo-spherical flow. No tests with coded flow regimes lower than 1.5 were interpreted for these tests. It is recalled that the GRF concept implemented in AQTESOLV is restricted to $n_{GRF} \leq 3$.

In Figure 3-14, the distributions of the estimated flow dimensions from standard analysis and GRF analysis in KFM03A are shown. Both analysis methods show that a flow dimension of 2±0.25 (pseudo-radial flow) is dominating. It should be noted that there are no tests with a flow dimension less than 0.75 (apparent no-flow boundaries) in this borehole. However, a number of test have flow dimensions greater than 2.5.

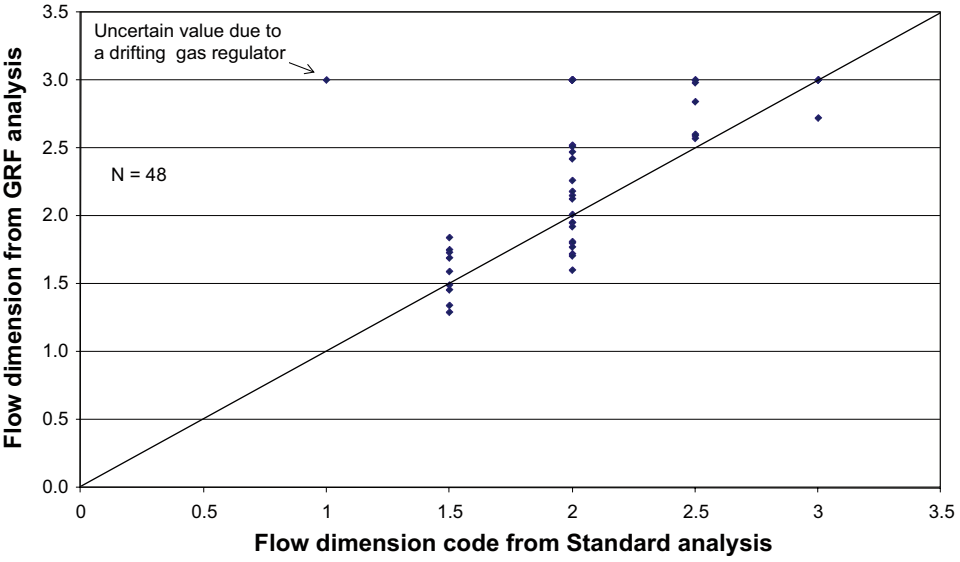

Figure 3-13. *Comparison of estimated flow dimensions from standard analysis and GRF analysis of 48 constant-head injection tests in KFM03A.*

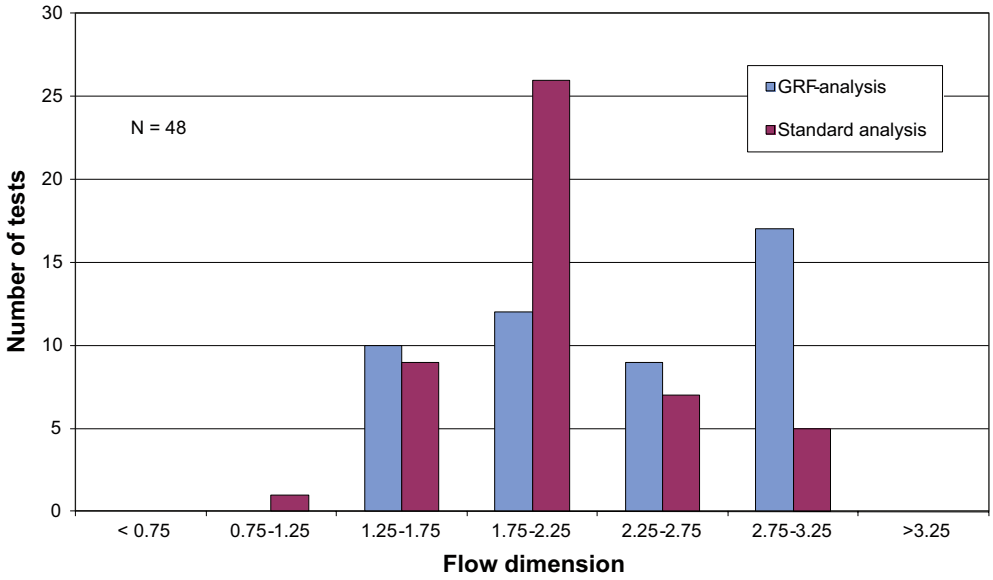

Figure 3-14. *Distribution of estimated flow dimensions from standard analysis and GRF analysis of 48 constant-head injection tests in KFM03A.*

The cumulative distribution of the estimated flow dimensions from the GRF analysis of the tests in KFM03A is shown in Figure 3-15. The figure shows that the median value of n_{GRF} of the 48 tests is close to 2.5, a value that suggests a pseudo-spherical flow regime.

Figure 3-16 shows a cross-plot of estimated transmissivities from GRF analysis (T_{GRF}) versus the best-choice transmissivities from the standard analysis (T_{BC}) of the selected constant-head injection tests in KFM03A. The figure indicates a fairly good agreement between T_{GRF} and T_{BC} in most cases in this borehole. Noteworthy, a large number of transmissivity values in KFM03A are smaller than $5 \cdot 10^{-8}$ m^2/s, which suggests that the flowing fractures are not particularly transmissive.

Figure 3-17 shows a scatter plot of the estimated GRF flow dimensions, n_{GRF}, from the injection period of the tests versus the observed pressure recovery (fraction) at the end of the recovery period in borehole KFM03A. The final pressure recovery is calculated as the percentage of the final recovery of the applied injection head in relation to the total injection head at the end of the recovery period. The figure shows that the final pressure recoveries are, in general, rather high in this borehole except in a few low-transmissive sections.

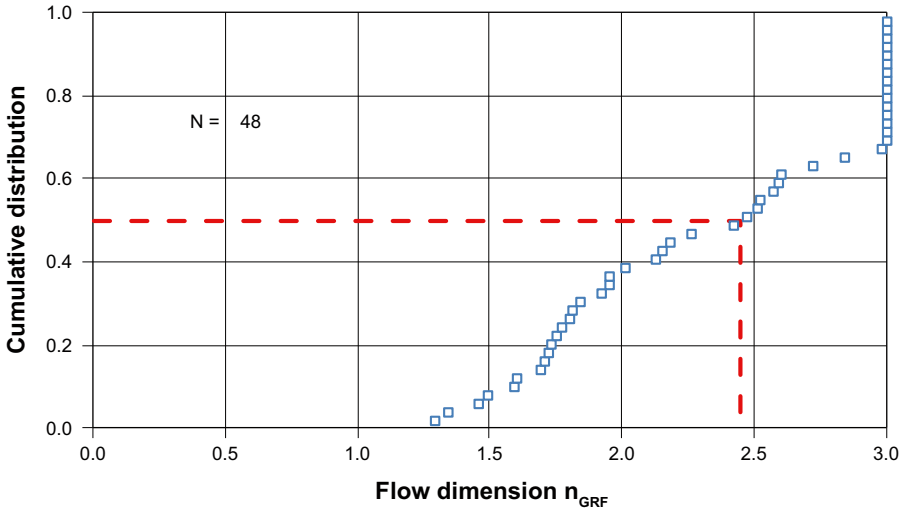

Figure 3-15. *Cumulative distribution of the estimated flow dimensions from GRF analysis of 48 constant-head injection tests in KFM03A.*

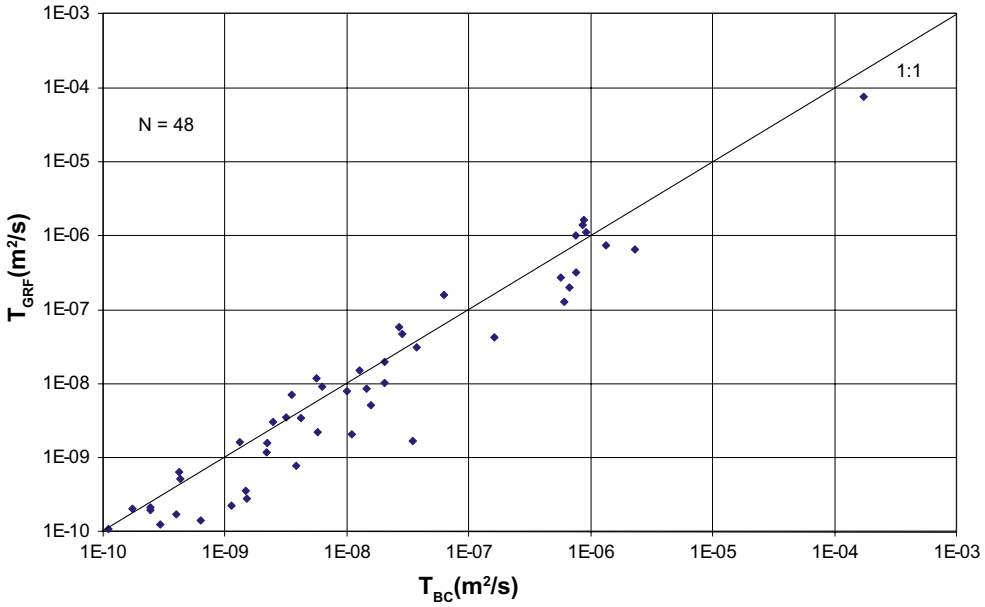

Figure 3-16. *Cross-plot of estimated transmissivities from GRF analysis (T_{GRF}) versus the best-choice transmissivities (T_{BC}) from the standard analysis in KFM03A.*

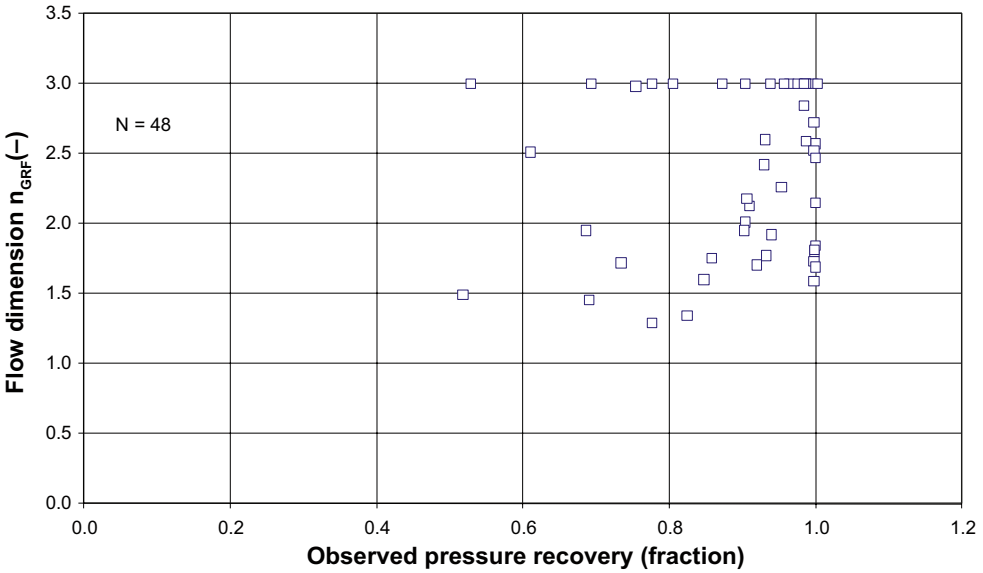

Figure 3-17. *Scatter plot of estimated flow dimensions from GRF analysis (n_{GRF}) versus the observed pressure recovery (fraction) for the same tests as in the previous figure in KFM03A.*

Figure 3-18 shows a cross-plot of the sum of estimated PFL fracture transmissivities (ΣT_{PFL}) versus the best-choice transmissivities (T_{BC}) from the standard analysis of the selected constant-head tests in KFM03A. Sections in which no conductive fractures could be detected in the PFL measurements are plotted at an arbitrary low value on the ordinate axis. The figure shows general good agreement between the lumped PFL fracture transmissivities and the PSS injection test transmissivities. In some test sections with T_{BC} below c $1 \cdot 10^{-8}$ m²/s from the injection tests, no conductive fractures could be detected by difference flow logging. Some of these sections show rather small recovery, indicating isolated fractures. The lowest value of the sum of ΣT_{PFL} is c $1 \cdot 10^{-9}$ m²/s in this borehole. As previously mentioned, values of ΣT_{PFL} above the 1:1 slope are probably due to different measurement, interpretation or methodological uncertainties, e.g. due to double-counting in the calculation of ΣT_{PFL}. This would occur if two or more intersecting fractures within a 5-m test interval merge to a single fracture away from the borehole.

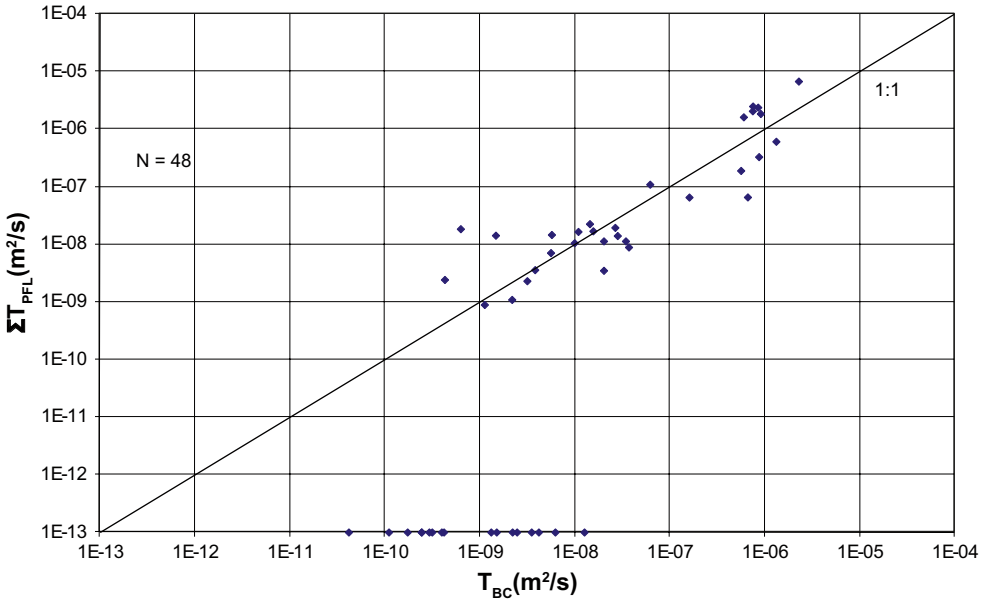

Figure 3-18. *Cross-plot of the sum of PFL fracture transmissivities (ΣT_{PFL}) versus the best-choice transmissivities (T_{BC}) from the standard analysis of 48 constant-head injection tests in KFM03A.*

3.7 Sections with low flow dimensions and poor pressure recovery

Measured and interpreted properties of the identified test sections with low interpreted GRF dimensions and observed low final pressure recovery in boreholes KFM03A and KFM06A are summarised in Table 3-3. As pointed out above the estimated T_{GRF} are uncertain in some tests with low flow dimensions.

Table 3-3. Interpreted flow dimensions, observed pressure recovery and estimated transmissivities of sections with low GRF dimensions and low pressure recovery in boreholes KFM03A and KFM06A.

Borehole section (m)	Flow regime code	n_{GRF}	Pressure recovery (fraction)	T_M (m^2/s)	T_{BC} (m^2/s)	T_{GRF} (m^2/s)	$\sum T_{PFL}$ (m^2/s)
KFM06A:220.5–225.5	1.5	1.25	0.73	$1.1\cdot10^{-6}$	$2.0\cdot10^{-7}$	$5.9\cdot10^{-6}$	$8.9\cdot10^{-8}$
KFM06A:250.5–255.5	0.5	0.28	0.22	$1.8\cdot10^{-8}$	$2.3\cdot10^{-8}$	$1.0\cdot10^{-5}$	$8.6\cdot10^{-10}$
KFM06A:290.5–295.5	0.5	0.63	0.53	$1.6\cdot10^{-9}$	$2.0\cdot10^{-9}$	$1.0\cdot10^{-5}$ *	<meas. limit
KFM06A:295.5–300.5	0.5	0.68	0.13	$1.6\cdot10^{-7}$	$5.1\cdot10^{-7}$	$3.9\cdot10^{-4}$ *	$2.2\cdot10^{-8}$
KFM06A:305.5–310.5	0.5	0.10	0.12	$7.4\cdot10^{-8}$	$7.4\cdot10^{-8}$	$7.8\cdot10^{-5}$ *	$2.1\cdot10^{-8}$
KFM06A:390.5–395.5	1.0	0.83	0.34	$3.0\cdot10^{-7}$	$7.2\cdot10^{-8}$	$8.1\cdot10^{-6}$	$2.4\cdot10^{-8}$
KFM03A:691–696	1.5	1.46	0.69	$6.1\cdot10^{-9}$	$6.2\cdot10^{-9}$	$9.3\cdot10^{-9}$	<meas. limit
KFM03A:721–726	1.5	1.29	0.78	$4.3\cdot10^{-9}$	$3.5\cdot10^{-9}$	$7.2\cdot10^{-9}$	<meas. limit

* uncertain value due to a low flow dimension.

The estimated transmissivities from GRF analysis (T_{GRF}) in most of the sections in KFM06A in Table 3-3 are significantly higher compared to those from the standard analysis while the lumped transmissivities from difference flow logging (ΣT_{PFL}) in most cases are much lower (sometimes even below the measurement limit). The rather low-transmissive test sections in KFM03A in Table 3-3 show the same pattern but less pronounced. For some tests with the lowest flow dimensions, the standard concept of transmissivity may be questioned. Such tests may correspond to isolated fracture(s) or flow channels. Concerning the tests in KFM06A, T_{BC} was chosen from the recovery period in all cases except for section 305.5–310.5 m for which the steady-state transmissivity T_M was chosen.

4 Discussion and conclusions

4.1 Comparison between standard and GRF well test interpretations

4.1.1 Flow dimension

The investigation analyses 151 constant-head injection tests in three cored boreholes at Forsmark (58 in KFM06A, 45 in KFM02A, and 48 in KFM03A). The estimated flow dimensions from standard well test analysis and GRF analysis give consistent results, see e.g. Figure 3-1 and Figure 3-2. This suggests that the assignment of flow dimension codes to the flow regimes identified by means of standard well test analysis go well together with the flow dimension concept defined in the GRF analysis. Hence, in this regard there is no additional conceptual information gained from using the GRF concept.

4.1.2 Test interval transmissivity

Geier et al. (1996) conclude that any type of well test interpretation uses simplistic fundamental assumptions, in the form of a simplified model of the conduit being tested, which allows for a reasonably unique determination of the model parameters. For the GRF approach, a particular assumption is that of homogeneity of the system. That is, flow dimension is assumed to be a homogeneous, constant feature of the test. Indeed, one would expect the flow dimension to be variable in a heterogeneous system. Wei and Charkabarty (1996) note that in fractured crystalline rock, a non-integer flow dimension could be caused by flow conduit geometry and/or property variations in the radial direction of a well test, and that we cannot differentiate between these two possibilities by a hydrogeological test alone.

For the sake of the objectives of the work reported here, a generalised radial flow transmissivity T_{GRF} has been calculated by means type curve fitting of the response curve (and its derivative) to the domination flow period during injection. The calculated values are cross-plotted versus T_{BC}. As expected, Figure 3-4 indicates that the largest deviations between T_{BC} and T_{GRF} for the selected constant-head injection tests in KFM06A occur for a number of test intervals with very low flow dimensions. As the flow dimension approaches zero the ratio T_{GRF}/T_{BC} could become very high, see Figure 4-1. For values of the flow dimension greater than two, T_{GRF} is lower than T_{BC} but the deviations are not as high as for small flow dimensions. This is simply a consequence of the dimension. For a given specific capacity, a higher dimension will give a lower T than 2-D flow and a lower dimension will give a higher T value.

In conclusion, the results suggest that the transmissivities derived with standard constant-head injection well test analysis methods and with the GRF concept, respectively, are similar provided that the dominating flow geometry during the testing is radial (cylindrical). Having flow geometries with dimensions other than 2 strongly affects the transmissivity value. For example, a flow system with a dimension of 1 may require an order of magnitude or more, higher transmissivity to produce the same flow rates.

The median of the GRF flow dimensions of all constant-head injection tests is 2.06 with 33% of the data in the range 1.75–2.25 and 40% of the data in range 2.25–3.00. It is noted that transmissivity is by definition a two-dimensional quantity and that it is not a useful quantity for flow dimensions less than 1 and greater than 3. If tests with flow dimensions less than 1 are excluded, which was the interpreted flow dimension for 11 tests or 7% of the data, the median changes to 2.16 with 35% of the in the range 1.75–2.25 and 44% of the data in the range 2.25–3.00.

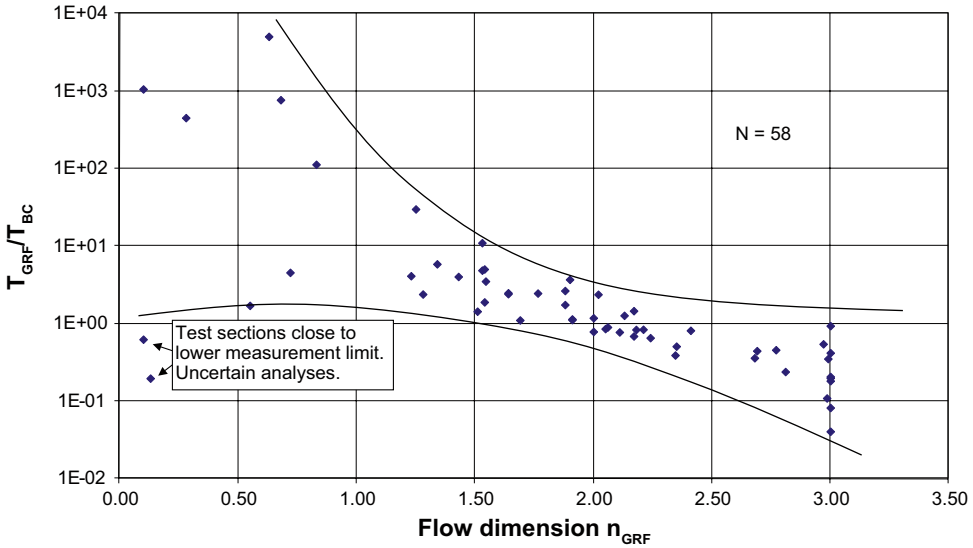

Figure 4-1. *Cross-plot of the transmissivity ratio T_{GRF}/T_{BC} versus the estimated flow dimension for the selected constant-head injection tests in KFM06A. The clustered values for nGRF = 3 correspond to the upper limit of nGRF in AQTESOLV. The two outliers towards the lower left corner correspond to two test sections close to the lower measurement limit of the injection tests and the analyses are thus very uncertain.*

4.1.3 Sections with low flow dimensions and poor pressure recovery

The observed pressure recoveries from PSS constant-head injection test reported here indicate that the conditions vary significantly between the studied boreholes, see the scatter plots in Figure 3-5, Figure 3-11, and Figure 3-17:

- In borehole KFM02A (Figure 3-11) almost all constant-head injection tests reveal a full pressure recovery. This is to be expected as the analysed sections in this borehole are mainly located within the interpreted possible deformation zones. These are denoted DZ2–DZ6 in Figure A-2 in Appendix A. The most prominent of these possible deformation zones is DZ6, which corresponds to the thick gently dipping fault zone ZFMA2, see SKB (2005) for details.
- In borehole KFM06A (Figure 3-5) a large number of the constant-head injection tests reveal a poor recovery, particularly those with low flow dimensions, n_{GRF}. KFM06A is located in the sparsely fractured footwall bedrock of the gently dipping deformation zone ZFM02A. Few of the analysed test intervals coincide with the possible deformation zones shown in Figure A-1 in Appendix A.
- In borehole KFM03A (Figure 3-17) the majority of the constant-head injection tests reveal a pressure recovery of 60% or better. Few of the analysed test intervals coincide with the possible deformation zones shown in Figure A-3 in Appendix A. Noteworthy, a large number of transmissivity values in KFM03A are smaller than $5 \cdot 10^{-8}$ m^2/s (Figure 3-16), which suggests that the flowing fractures are not particularly transmissive.

4.2 Differences between PSS and PFL measurements as applied in the site characterisation

It is concluded that it is not always the interconnected open fractures only that are detected and analysed with the PSS method. The transmissivities of isolated fractures or isolated clusters of fractures, connected to the test interval may also be measured with the PSS method. In order to resolve the connectivity away from the borehole, it is concluded that the duration of the constant-head injection tests must be longer than the 20 minutes used in SKB's site investigation programme. In comparison, isolated fractures or isolated clusters of fractures connected to the pumped borehole are not investigated with the PFL method; that is, only connected open fractures with a sufficient flow rate after several days of pumping can be detected with the PFL method.

The difference in hydraulic characterisation using the PSS method and the PFL method is schematically shown in Figure 4-2. The constituent quantities measured where the fractures intersects the borehole are the flow rate Q and the pressure difference Δp. Since these quantities are coupled, the key parameter of importance is the specific capacity Q/Δp. The specific capacity is dependent on:

- Q_{limit}; the lower measurement limit of the test method.
- T_{bh}; the local transmissivity where the borehole penetrates a heterogeneous fracture. In a two-shell composite, the apparent transmissivity is dominated by the lower value T shell (Follin 1992).
- C; the connectivity of the fractures intersecting the borehole to other fractures away from the borehole. Some fractures are isolated, or a part of an isolated cluster of fractures. Others, in turn, are part of the overall hydrological system.
- T/S; the hydraulic diffusivity of the fracture system.
- t; the duration of the hydraulic testing, i.e. the test time.
- ΔL; the length of the test interval (test section).

All Cases A–F in Figure 4-2 are possible to observe with the PSS method, including compartmentalised fracture network situations such as Cases A–C. The PFL method, however, can only detect flowing connected open fractures above the lower measurement limit, i.e., it would only detect flow for Cases D–F.

Figure 4-3 shows cumulative distributions of T_{BC}, T_{GRF} and ΣT_{PFL} for the 49 test intervals in KFM06A that have flow dimensions, n_{GRF}, between 1 and 3. The plot shows very similar cumulative distributions for T_{BC} and T_{GRF} throughout the 49 test intervals. Further, the deviations between the PSS and PFL methods start at the 55% percentile, which appears at c $5 \cdot 10^{-8}$ m^2/s. Thus, in the high end the inferred transmissivity distributions are similar, whereas they are not in the low end.

Values of ΣT_{PFL} above the 1:1 slope in Figure 3-6, Figure 3-12, and Figure 3-18 are probably due to different measurement, interpretation or methodological uncertainties. For instance, there is a risk for double-counting in the calculation of ΣT_{PFL}. This would occur if two or more intersecting fractures within a 5-m test interval merge to a single fracture away from the borehole.

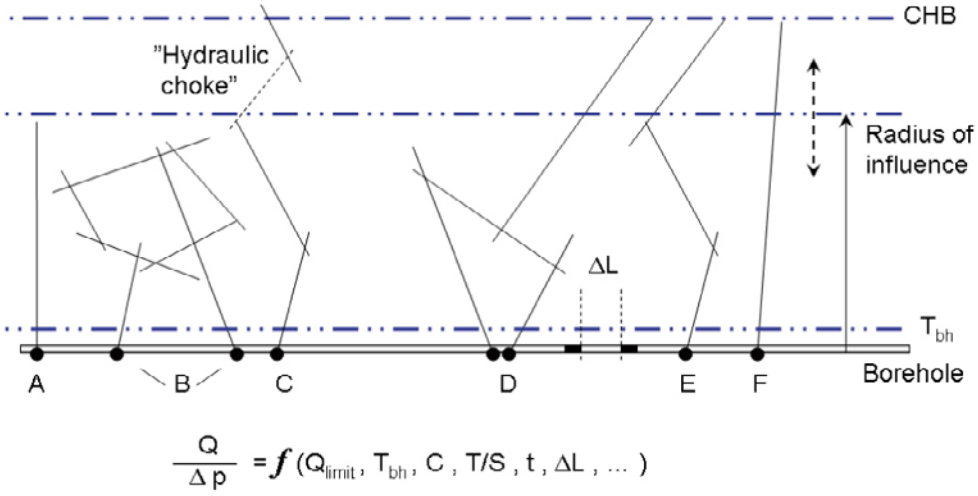

Figure 4-2. *Cartoon showing a borehole with six different symbolic fracture network situations, Cases A–F. Cases A–C represent isolated fractures/fracture networks and Cases D–F represent fracture networks connected to the overall hydrogeological system. The latter is here indicated by a "constant-head boundary" (CHB) suggesting a steady-state flow at long test times. The cartoon is rotated 90° to improve the readability. The notation shown in the figure is explained in the text.*

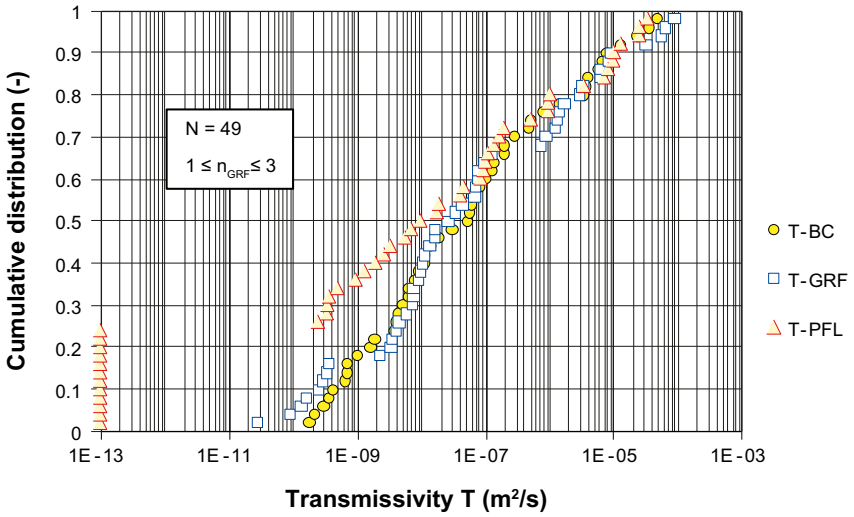

Figure 4-3. *Cumulative distributions of T_{BC}, T_{GRF} and ΣT_{PFL} for the analysed test intervals in KFM06A that have flow dimensions, n_{GRF}, between 1 and 3.*

4.3 On the usage of transmissivity data in groundwater flow modelling for the complete site investigation phase

During the initial site investigation phase, Follin et al. (2005) investigated the fracture connectivity of flowing fractures detected with the PFL method. The underlying principle of the connectivity analysis advocated by Follin et al. (2005) may be written as:

$$P_{10,all} \geq P_{10,open} \geq P_{10,cof} \geq P_{10,PFL} \qquad (4\text{-}1)$$

where P_{10} denotes fracture frequency (m^{-1}), a quantity that is determined by core mapping and down-hole borehole images using a televiewer. The different subscripts in (4-1) denote: all = *all fractures*, open = *all open fractures*, cof= *all connected open fractures*, and PFL = *all flowing connected open fractures above the lower measurement limit of the PFL method*, respectively. The four intensities are illustrated in Figure 4-1.

During the initial site investigation phase, Hartley et al. (2005) developed a procedure for the calibration of fracture intensity of DFN models by means of steady-flow pumping test simulations. Since the PFL method measures the specific capacity of a network of flowing fractures and not the fracture transmissivity of the intersecting fracture, the results from these simulations were compared with the histogram of specific capacities measured with the PFL method. Three different kinds of correlations between fracture transmissivity, T (m^2/s), versus fracture size, r (m), were tested; correlated, semi-correlated and uncorrelated:

$$T = a\, r^{\,b} \qquad (4\text{-}2)$$

$$T = 10^{\,(\log(a\, r\hat{}b) + \sigma\_\log(T)\, N(0,1))} \qquad (4\text{-}3)$$

$$T = 10^{\,N(\mu\_\log(T),\sigma\_\log(T))} \qquad (4\text{-}4)$$

where N(0,1) denotes a normally distributed random deviate of mean 0 and a standard deviation of 1.

For the complete site investigation phase it is suggested that the connectivity analysis suggested by Follin et al. (2005) is used together with the procedure for calibration of fracture intensity by means of pumping test simulations developed by Hartley et al. (2005). Besides comparing simulated and measured specific capacities at steady-state radial flow it could perhaps be of value to also explore the flow dimensions using a transient radial flow model. However, this requires a model for the fracture storativity.

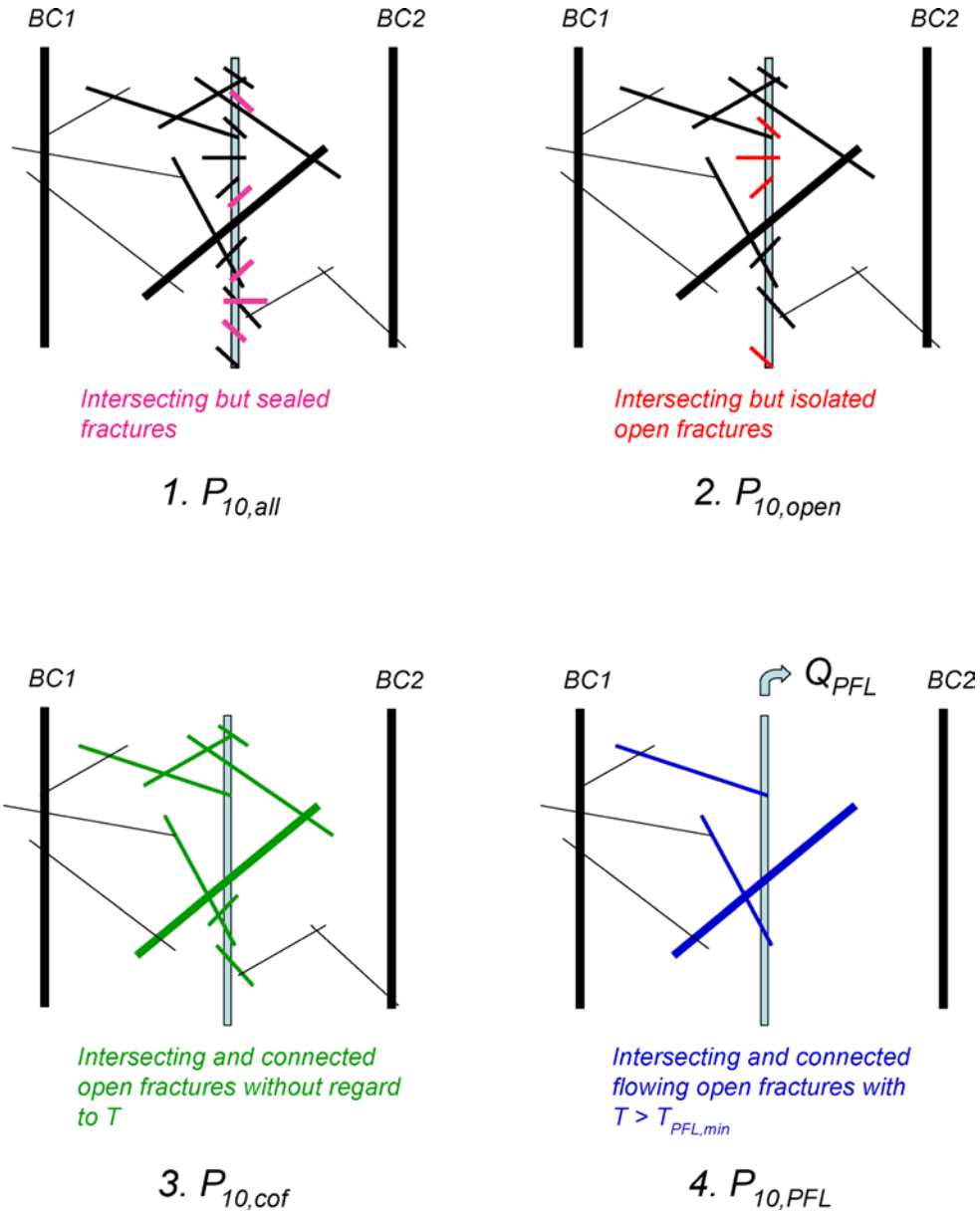

Figure 4-4. *1) $P_{10,all}$ is the frequency of all fractures intersecting the borehole, 2) $P_{10,open}$is the frequency of "all open fractures", c) $P_{10,cof}$ of is the frequency of "all connected open fractures", and 4) $P_{10,PFL}$ is the frequency of " all interconnected, open, flowing fractures that have a transmissivity greater than the lower detection limit" (c. $1 \cdot 10^{-9}$ m^2/s). BC1 and BC2 represent constant head boundaries. Modified after Figure 5-6 in Follin et al. (2005).*

5 References

SKB's (Svensk Kärnbränslehantering AB) publications can be found at www.skb.se/publications.

Almén K-E, Andersson O, Fridh B, Johansson B-E, Sehlstedt M, Gustafsson E, Hansson K, Olsson O, Nilsson G, Axelsen K, Wikberg, P, 1986a. Site investigation. Equipment for geological, geophysical, hydrogeological and hydrochemical characterization. SKB TR 86-16, Svensk Kärnbränslehantering AB.

Almén K-E, Andersson J-E, Carlsson L, Hansson K, Larsson N-Å, 1986b. Hydraulic testing in crystalline rock. A comparative study of single-hole test methods. SKB TR 86-27, Svensk Kärnbränslehantering AB.

Barker J A, 1988. A generalized radial flow model for hydraulic tests in fractured rock. Water Resources Research, 24, pp 1796–1804.

Black J H, Barker J A, 1987. Design of single-borehole hydraulic test programme allowing for interpretation-based errors. Nagra Technical Report NTB 87-03, National Cooperative for the Disposal of Radioactive Waste, Switzerland.

Braester C, Thunvik R, 1982. Numerical simulation of double-packer tests. Calculation of rock permeability. SKB TR 82-06, Svensk Kärnbränslehantering AB.

Braester C, Thunvik R, 1984. Determination of formation permeability by double-packer tests. Journal of Hydrology, 72, pp 375–389.

Doe T, 2002. Äspö Hard Rock Laboratory. TRUE Block Scale Project. Generalized dimension analysis of build-up and pressure interference tests. SKB IPR-02-70, Svensk Kärnbränslehantering AB.

Doe T W, Geier J E, 1990. Interpretation of fracture system geometry using well test data. SKB Stripa Project Technical Report 91-03, Svensk Kärnbränslehantering AB.

Dougherty D E, Babu D K, 1984. Flow to a partially penetrating well in a double-porosity reservoir. Water Resources Research, 20, pp 1116–1122.

Earlougher R C, 1977. Advances in well test analysis. New York: Society of Petroleum Engineers of AIME. (Henry L. Doherty Series 5).

Follin S, 1992. On the interpretation of double-packer tests in heterogeneous porous media: Numerical simulations using the stochastic continuum analogue. SKB TR 92-36, Svensk Kärnbränslehantering AB.

Follin S, Stigsson M, Svensson U, 2005. Regional hydrogeological simulations for Forsmark – numerical modelling using DarcyTools. Preliminary site description Forsmark area – version 1.2. SKB R-05-60, Svensk Kärnbränslehantering AB.

Forssman I, Zetterlund M, Rhén I, 2004. Forsmark site investigation. Correlation of Posiva Flow Log anomalies to core mapped features in KFM01A to KFM05A. SKB R-04-77, Svensk Kärnbränslehantering AB.

Fransson Å, 2002. Nonparametric method for transmissivity distributions along boreholes. Ground Water, 40, pp 201–204.

Geier J E, Axelsson C-L, Hässler L, Benabderrahmane A, 1992. Discrete fracture modelling of the Finnsjön rock mass: Phase 2. SKB TR 92-07, Svensk Kärnbränslehantering AB.

Geier J E, Doe T W, Benabderrahmane A, Hässler L, 1996. SITE-94. Generalized radial flow interpretation of well tests for the SITE-94 Project. SKI Report 96:4, Statens Kärnkraftsinspektion (Swedish Nuclear Power Inspectorate).

Hantush M S, 1959. Nonsteady flow to flowing wells in leaky aquifers. Journal of Geophysical Research, 64, pp 1043–1052.

Hartley L, Cox I, Hunter F, Jackson P, Joyce S, Swift B, Gylling B, Marsic N, 2005. Regional hydrogeological simulations for Forsmark – numerical modelling using CONNECTFLOW. Preliminary site description Forsmark area – version 1.2. SKB R-05-32, Svensk Kärnbränslehantering AB.

Hjerne C, Ludvigson J-E, Lindquist A, 2005. Forsmark site investigation. Single-hole injection tests in borehole KFM06A and KFM06B. SKB P-05-165, Svensk Kärnbränslehantering AB.

Hurst W, Clark J D, Brauer E B, 1969. The skin effect in producing wells. Journal of Petroleum Technology, 21, pp 1483–1489.

Jacob C E, Lohman S W, 1952. Nonsteady flow to a well of constant drawdown in an extensive aquifer. Transactions, American Geophysical Union, 33, pp 559–569.

Källgården J, Ludvigson J-E, Hjerne C, 2004. Forsmark site investigation. Single-hole injection tests in borehole KFM03A. SKB P-04-194, Svensk Kärnbränslehantering AB.

Levén J, Carlberg T, Follin S, 2006. Forsmark site investigation. Compilation and visualisation of cross discipline borehole data using WellCad. Boreholes KFM01A–KFM07A. SKB P-06-55, Svensk Kärnbränslehantering AB.

Ludvigson J-E, Hansson K, Rouhiainen P, 2002. Methodology study of Posiva difference flow meter in borehole KLX02 at Laxemar. SKB R-01-52, Svensk Kärnbränslehantering AB.

Ludvigson J-E, Hansson K, Hjerne C, 2007. Forsmark site investigation. Method evaluation of single-hole hydraulic injection tests at site investigations in Forsmark. SKB P-07-80, Svensk Kärnbränslehantering AB.

Moye D G, 1967. Diamond drilling for foundation exploration. Civil Engineering Transactions, Institute of Engineers, Australia, CE9, pp 95–100.

Osnes J D, Winberg A, Andersson J-E, Larsson N-Å, 1991. Analysis of well test data – application of probabilistic models to infer hydraulic properties of fractures. Topical Report RSI-0338, RE/SPEC, Inc.

Pöllänen J, Sokolnicki M, 2004. Forsmark site investigation. Difference flow logging in borehole KFM03A. SKB P-04-189, Svensk Kärnbränslehantering AB.

Rhén I (ed), Gustafson G, Stanfors R, Wikberg P, 1997. Äspö HRL – Geoscientific evaluation 1997/5. Models based on site characterization 1986–1995. SKB TR 97-06, Svensk Kärnbränslehantering AB.

Rhén I, Follin S, Hermanson J, 2003. Hydrological Site Descriptive Model – a strategy for its development during Site Investigations. SKB R-03-08, Svensk Kärnbränslehantering AB.

Rouhiainen P, Pöllänen J, 2004. Forsmark site investigation. Difference flow logging in borehole KFM02A. SKB P-04-188, Svensk Kärnbränslehantering AB.

Rouhiainen P, Sokolnicki M, 2005. Forsmark site investigation. Difference flow logging in borehole KFM06A. SKB P-05-15, Svensk Kärnbränslehantering AB.

SKB, 2005. Preliminary site description. Forsmark area – version 1.2. SKB R-05-18, Svensk Kärnbränslehantering AB.

Svensson T, Ludvigson J-E, Hjerne C, 2005. Forsmark site investigation. Single-hole injection tests in borehole KFM02A, re-measurements after hydraulic fracturing. SKB P-05-145, Svensk Kärnbränslehantering AB.

Theis C V, 1935. The relation between the lowering of the piezometric surface and the rate and duration of discharge of a well using ground-water storage. Transactions, American Geophysical Union, 16, pp 519–524.

Thiem G, 1906. Hydrologische Methoden, J M Gebhardt, Leipsig.

Walker D D, Roberts R M, 2003. Flow dimensions corresponding to hydrogeologic conditions. Water Resources Research, 39, 1349. doi:10.1029/2002WR001511.

Wei L, Chakrabarty C, 1996. Evaluation of a self-consistent approach to fractured crystalline rock characterization. Nuclear Science and Technology Report EUR 16926, European Commission.

Appendix A

Visualisation of cross-discipline borehole data in boreholes KFM06A, KFM02A and KFM03A

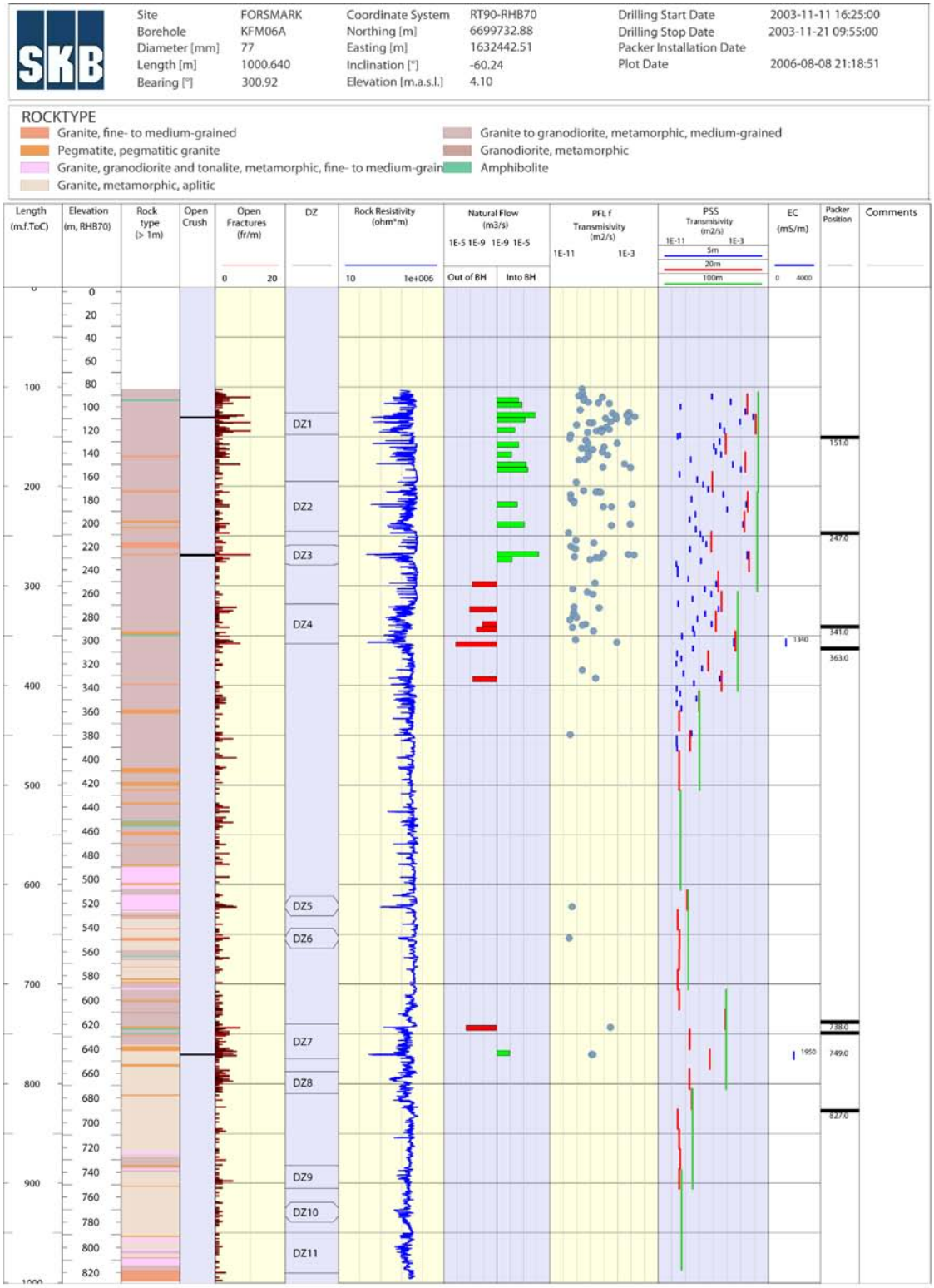

Figure A-1. *WellCad plot of multidisciplinary data in borehole KFM06A (Levén et al. 2006). Borehole KFM06A is located in the sparsely fractured footwall bedrock of the gently dipping deformation zone ZFMA2.*

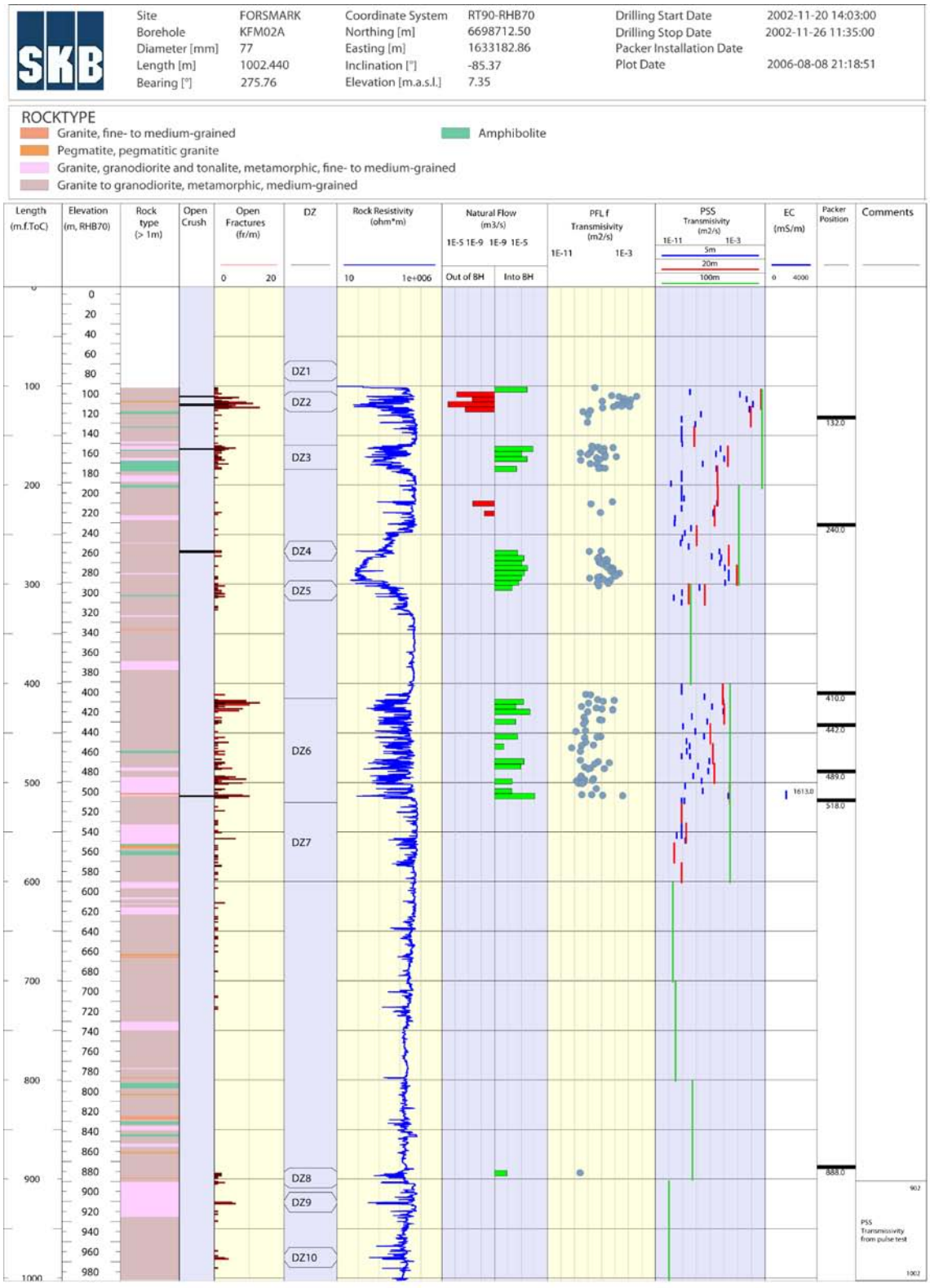

Figure A-2. *WellCad plot of multidisciplinary data in borehole KFM02A (Levén et al. 2006). DZ6 is the gently dipping deformation zone ZFMA2.*

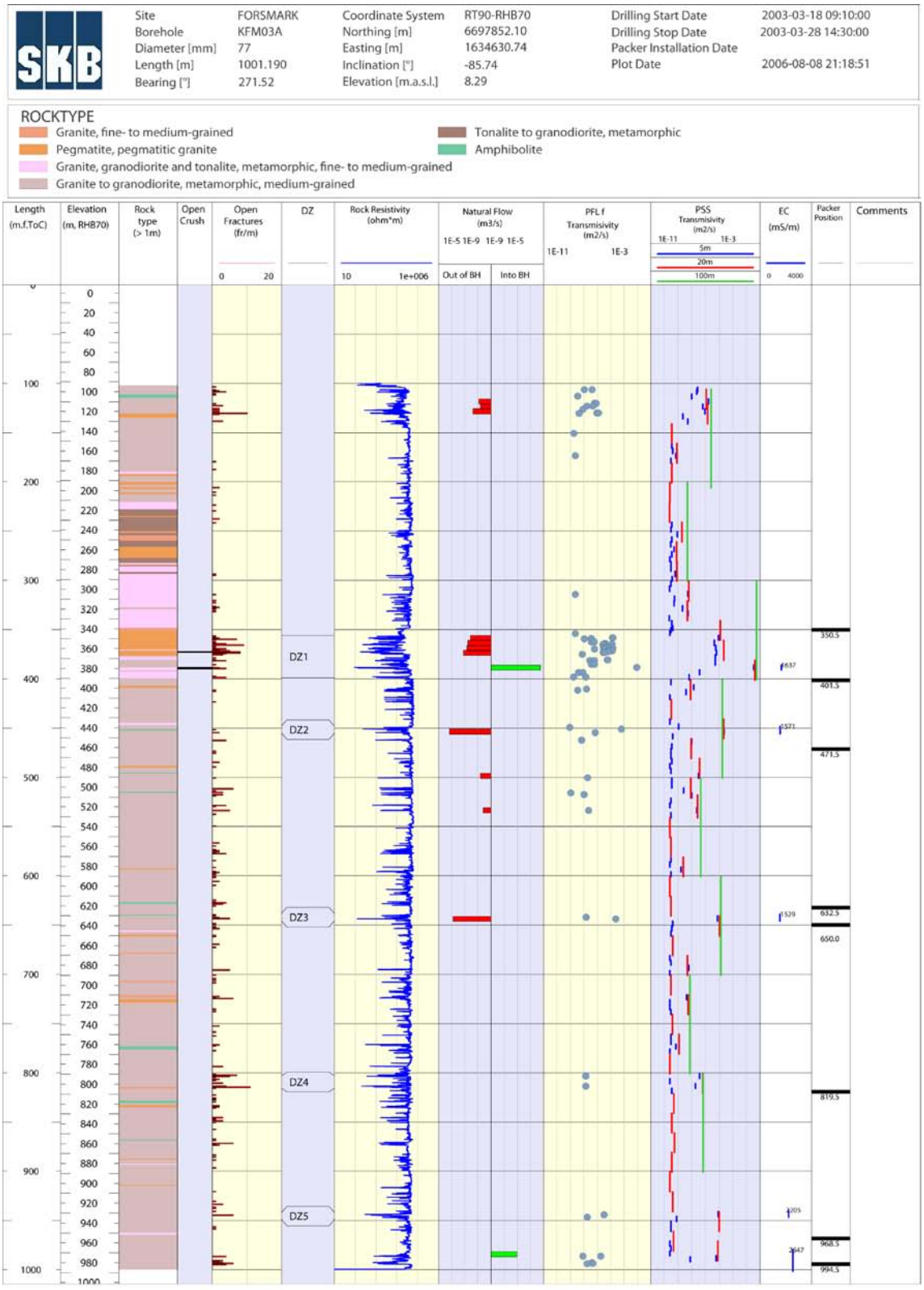

Figure A-3. *WellCad plot of multidisciplinary data in borehole KFM03A (Levén et al. 2006). Borehole KFM03A is located in the hanging wall bedrock of the gently dipping deformation zone ZFMA2.*

Appendix B

Comparison of radial and linear flow calculations

Figure B-1 compares the hydraulic conductivity values given by the specific capacity and the steady cylindrical solution (Thiem's equation) and the steady linear solution (Darcy's law). The two calculations use the same aquifer surface areas at the borehole and the same radii of influence. The conductivities differ by nearly two orders of magnitude.

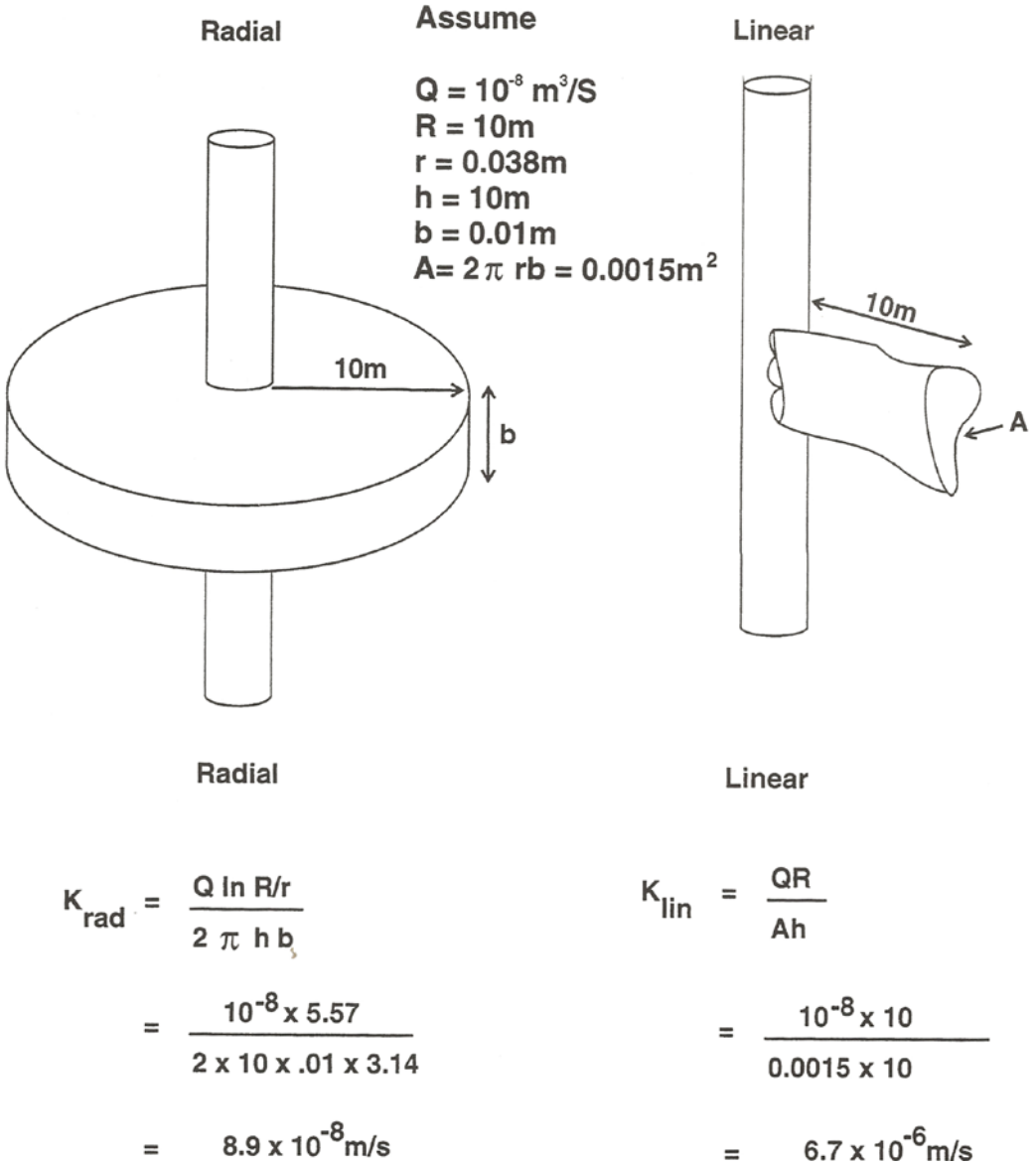

Figure B-1. *Comparison of radial and linear flow calculations. Reproduced from Wei and Chakrabarty (1996).*

Appendix C

Comparison between standard analysis and GRF analyses of injection tests in four selected 5-m test intervals in KFM06A

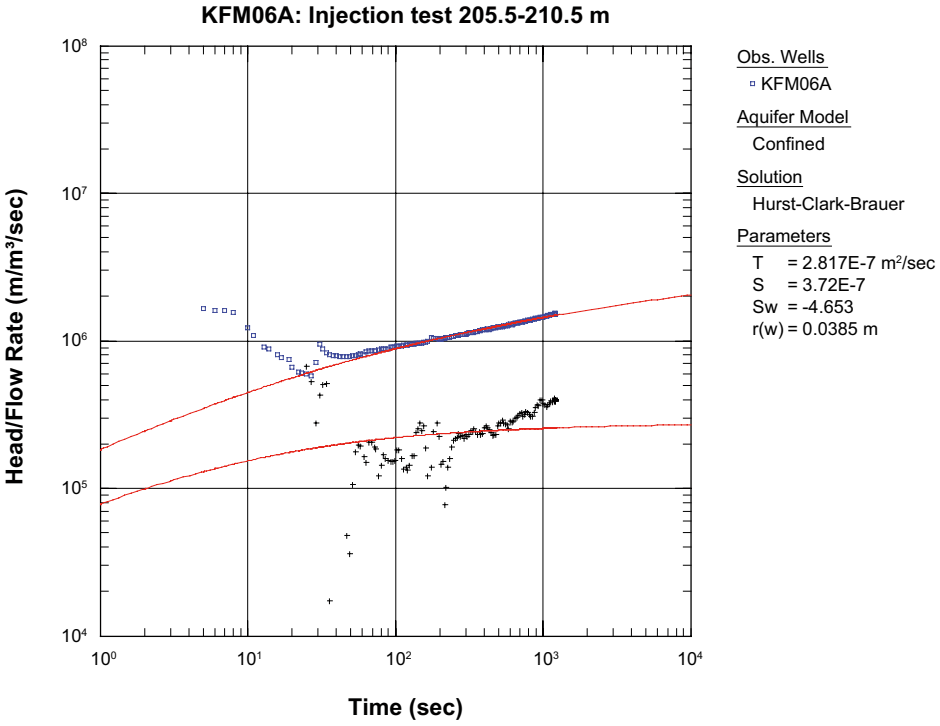

Figure C-1a. *Standard analysis log-log plot of head/flow rate (blue□) and derivative (black+) versus time together with corresponding best-fit type curves (red lines) from the injection period in test section KFM06A:205.5–210.5 m.*

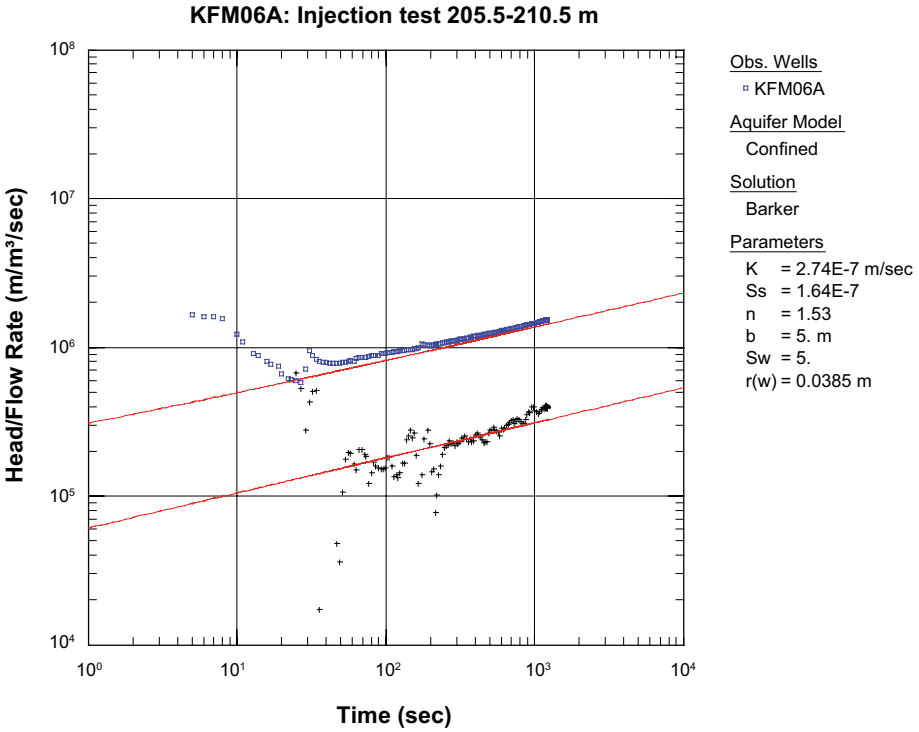

Figure C-1b. *Same test section as above. Example of approximate GRF analysis with a flow dimension n_{GRF} less than 2.*

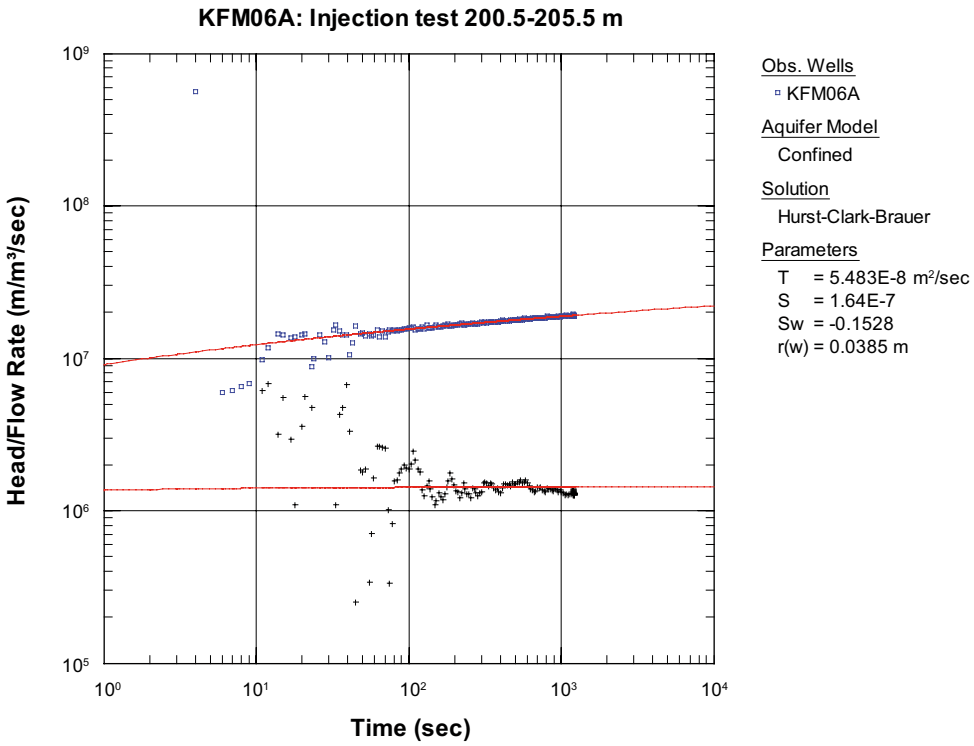

Figure C-2a. *Standard analysis log-log plot of head/flow rate (blue□) and derivative (black+) versus time together with corresponding best-fit type curves (red lines) from the injection period in test section KFM06A:200.5–205.5 m.*

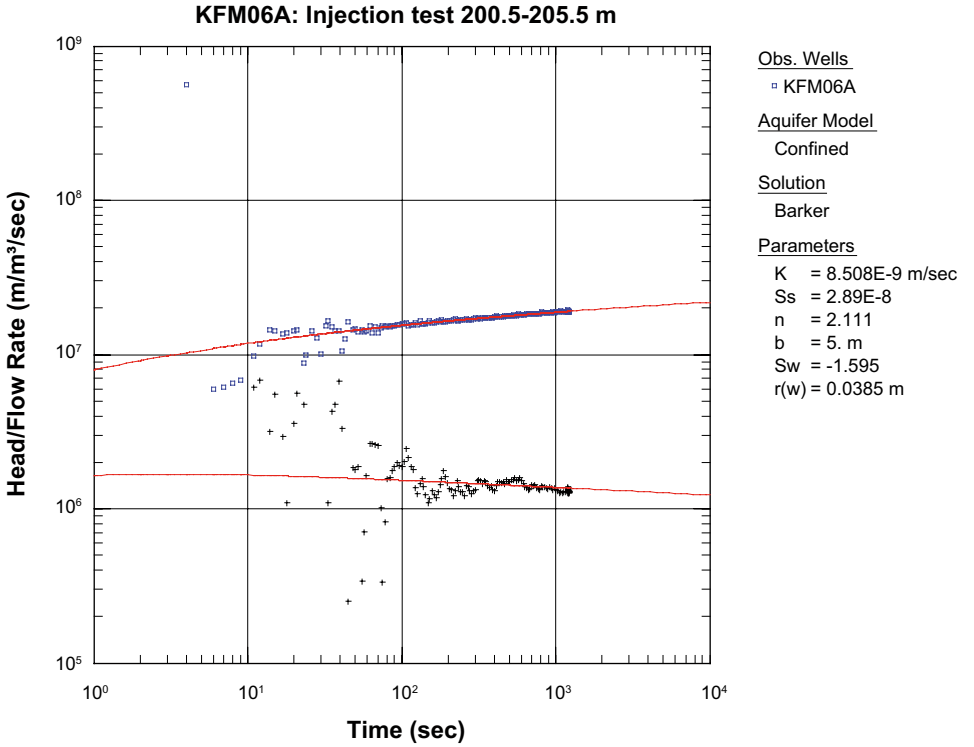

Figure C-2b. *Same test as above. Example of GRF analysis with a flow dimension n_{GRF} close to 2.*

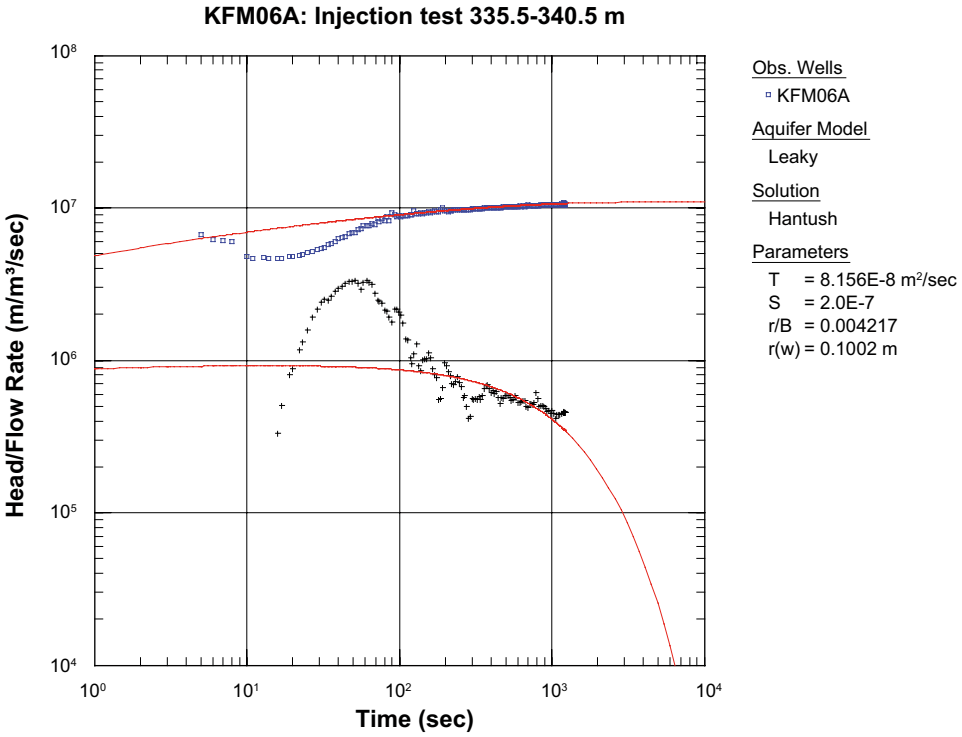

Figure C-3a. *Standard analysis log-log plot of head/flow rate (blue□) and derivative (black+) versus time together with corresponding best-fit type curves (red lines) from the injection period in test section KFM06A:335.5–340.5 m.*

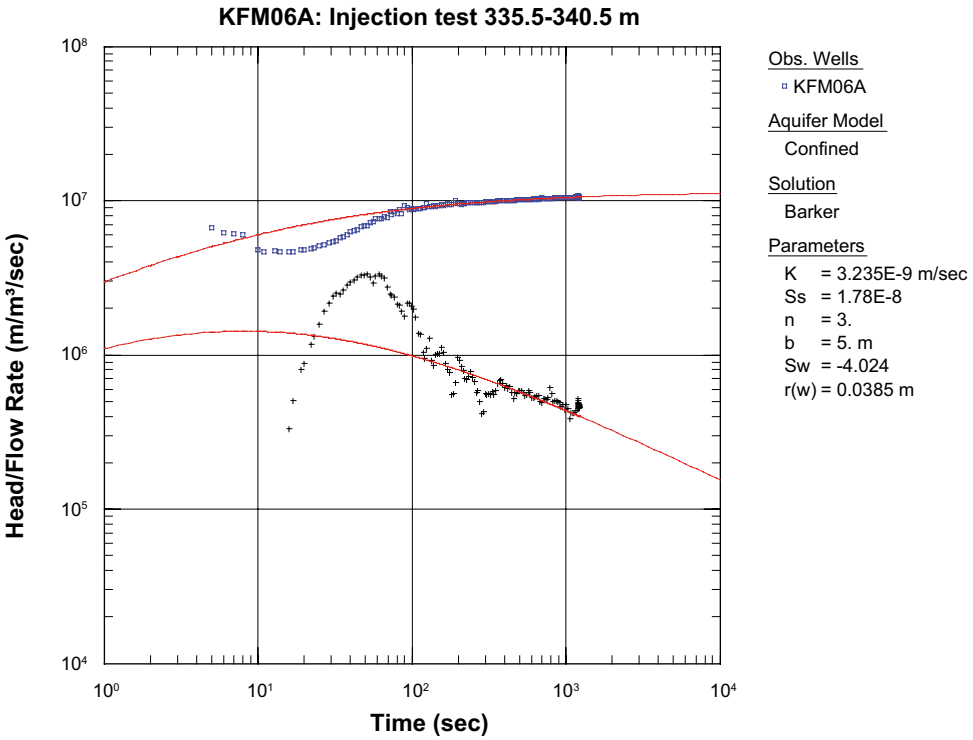

Figure C-3b. *Same test section as above. Example of GRF analysis with a flow dimension n_{GRF}=3.*

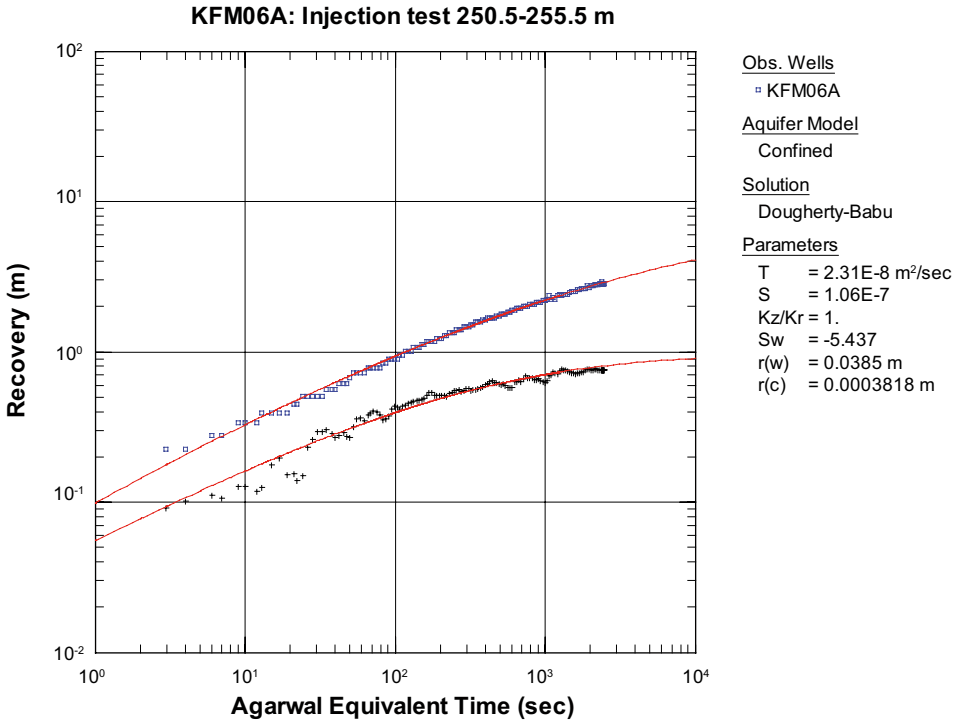

Figure C-4a. *Standard analysis log-log plot of pressure recovery (blue□) and derivative (black+) versus equivalent time together with corresponding best-fit type curves (red lines) from the* ***recovery*** *period in test section KFM06A:250.5–255.5 m. No unambiguous transient analysis could be made from the injection period using the standard analysis.*

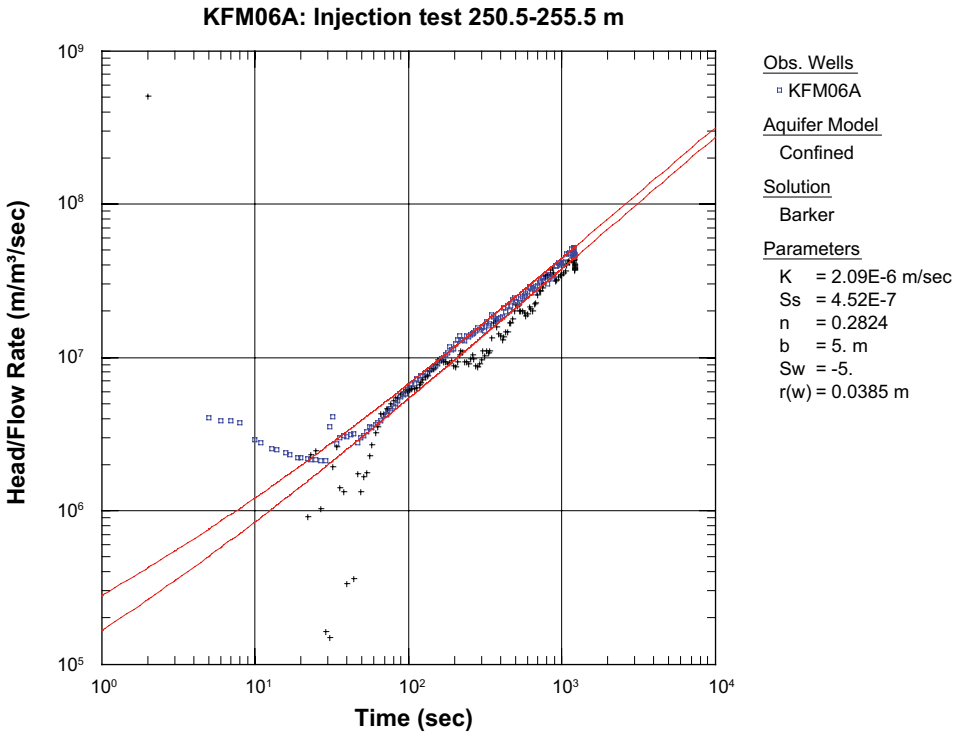

Figure C-4b. *Log-log plot of head/flow rate (blue□) and derivative (black+) versus time together with corresponding simulated curves (red lines) from the* ***injection*** *period of the same test section as above. Example of approximate GRF analysis with a very low flow dimension* n_{GRF}.

Table C-1. Compilation of hydraulic properties in AQTESOLV for the four 5-m intervals shown in Figure C-1a to Figure C-4b. The corresponding transmissivity values from the difference flow logging using the PFL method (ΣT_{PFL}) and the number of flowing fractures (N) are also shown. The symbols T, S and S_w are explained i Chapter 2 and the meaning of Code is explained in Section 3.2 and Table 3-1.

		Standard analysis				GRF analysis				PFL	
Borehole	Secup–Seclow	Code (–)	T (m^2/s)	S (–)	S_w (–)	n_{GRF} (–)	T_{GRF} (m^2/s)	S_{GRF} (–)	S_w (–)	N (–)	ΣT_{PFL} (m^2/s)
KFM06A	205.5–210.5	1.5[1]	$2.8\cdot10^{-7}$	$3.7\cdot10^{-7}$	–4.7	1.5	$1.4\cdot10^{-6}$	$8.2\cdot10^{-7}$	+5.0	4	$1.3\cdot10^{-7}$
KFM06A	200.5–205.5	2[1]	$5.5\cdot10^{-8}$	$1.6\cdot10^{-7}$	–0.2	2.1	$4.3\cdot10^{-8}$	$1.4\cdot10^{-7}$	–1.6	1	$3.2\cdot10^{-9}$
KFM06A	335.5–340.5	3[3]	$8.2\cdot10^{-8}$	$2.0\cdot10^{-7}$	–	3.0	$1.6\cdot10^{-8}$	$8.9\cdot10^{-8}$	–4.0	2	$6.7\cdot10^{-9}$
KFM06A	250.5–255.5	0.5[2]	$2.3\cdot10^{-8}$	$1.1\cdot10^{-7}$	–5.4	0.3	$1.0\cdot10^{-5}$	$2.3\cdot10^{-6}$	–5.0	1	$8.6\cdot10^{-10}$

[1] Confined, /Hurst et al. 1969/.
[2] Confined, /Dougherty and Babu 1984/.
[3] Leaky, /Hantush 1959/.